25.2 Surface composition

- **ultrahigh vacuum** (UHV), pressures lower than about 10^{-7} Pa.
- **escape depth,** the maximum depth from which ejected electrons come.
- **photoemission spectroscopy,** photoelectron spectroscopy applied to surfaces.
- **secondary-ion mass spectrometry** (SIMS), a technique in which a surface is ionized by bombardment with other ions and the secondary ions that emerge from the surface are detected by a mass spectrometer.

25.2 Surface composition (cont..)

- **reflection–absorption infrared spectroscopy** (RAIRS), a technique for obtaining the infrared absorption spectrum of the adsorbate.
- **surface-enhanced Raman scattering** (SERS), strong enhancement of the Raman spectrum of the adsorbate.
- **electron energy loss spectroscopy** (EELS or HREELS), a technique in which the energy loss suffered by a beam of electrons is monitored when they are reflected from a surface.
- **Auger electron spectroscopy** (AES), spectroscopy based on the Auger effect.

25.2 Surface composition (cont..)

- **reconstruction**, modification of the substrate surface layers in response to adsorbates.
- **low-energy electron diffraction** (LEED), electron diffraction by surfaces.
- **molecular beam scattering** (MBS), the scattering of a beam of adsorbate molecules by a surface.

Light-molecule interaction

The quantum mechanics interpretation

$$\hat{\mathcal{H}}(q,t) = \hat{H}(q) - \hat{\boldsymbol{\mu}} \cdot \hat{\mathbf{E}} = \hat{H}(q) + \hat{H}'(q,t)$$

where

$\hat{H}'(q,t)$ is the small time-dependent perturbation in the Hamitonian due to the light-molecule interaction

$\hat{\boldsymbol{\mu}} = \sum_i q_i \hat{\mathbf{r}}_i$ is the dipole moment of the molecule

$\hat{\mathbf{E}}$ is the electric field of the light

Molecular rotation

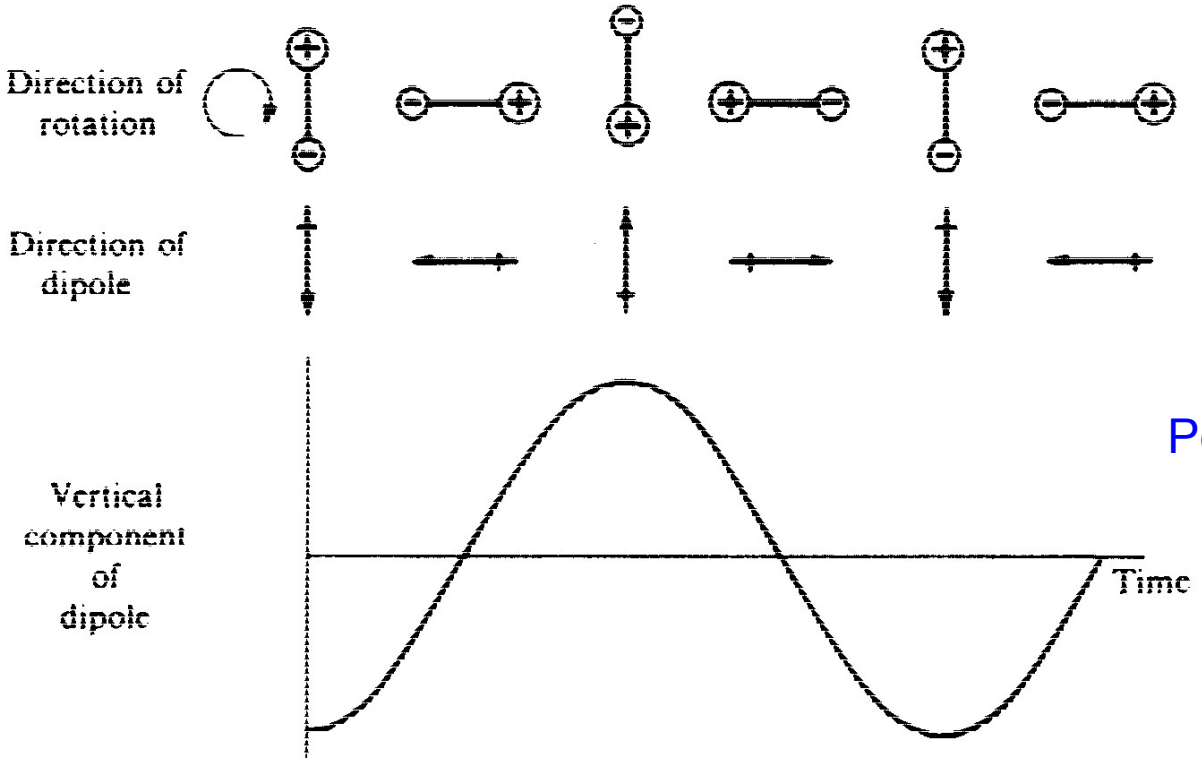

Figure 1.5 The rotation of a polar diatomic molecule, showing the fluctuation in the dipole moment measured in a particular direction

Permanent dipole moment:

$\hat{\mu} \neq 0$

C. N. Banwell & E. M. McCash, *Fundamentals of Molecular Spectroscopy* (1994)

Molecular vibrations

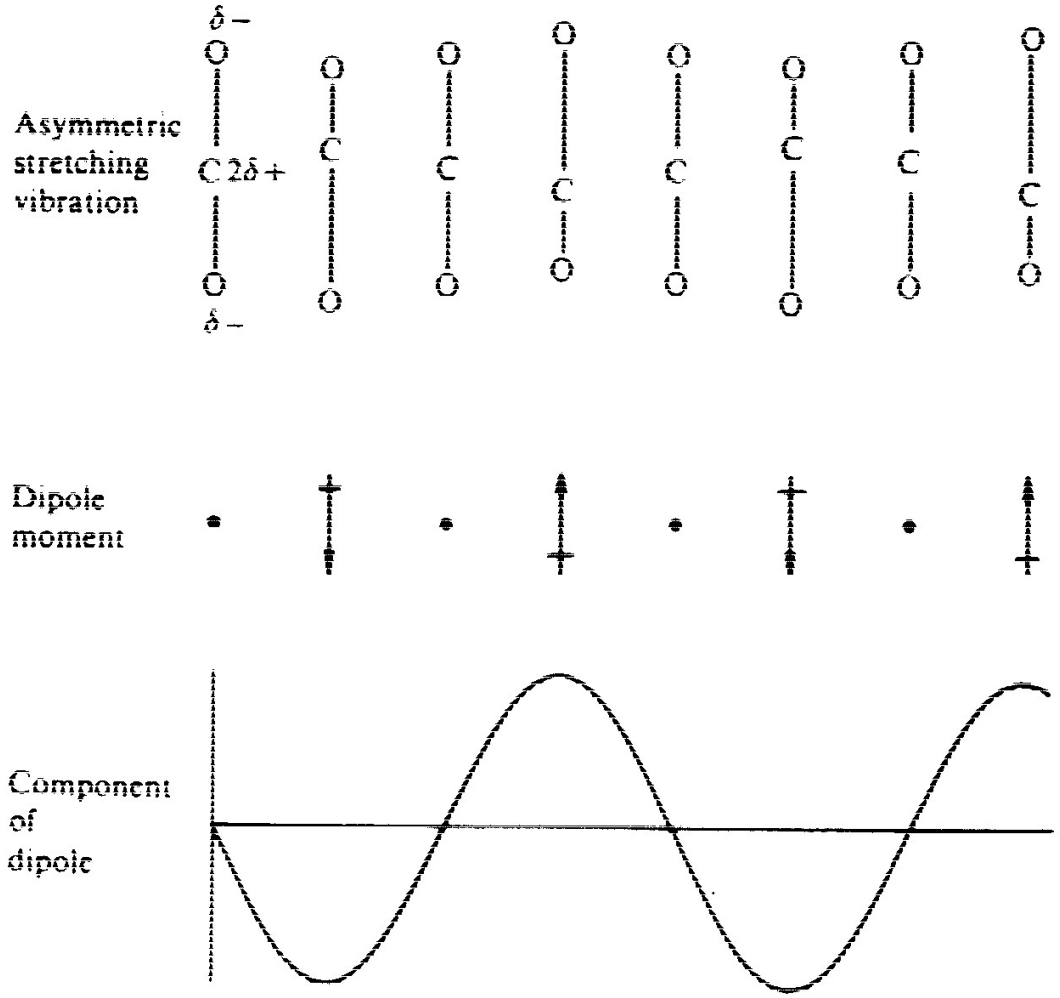

Transition dipole moment:

$\hat{\mu}' \neq 0$

IR active

Figure 1.7 The asymmetric stretching vibration of the carbon dioxide molecule, showing the fluctuation in the dipole moment.

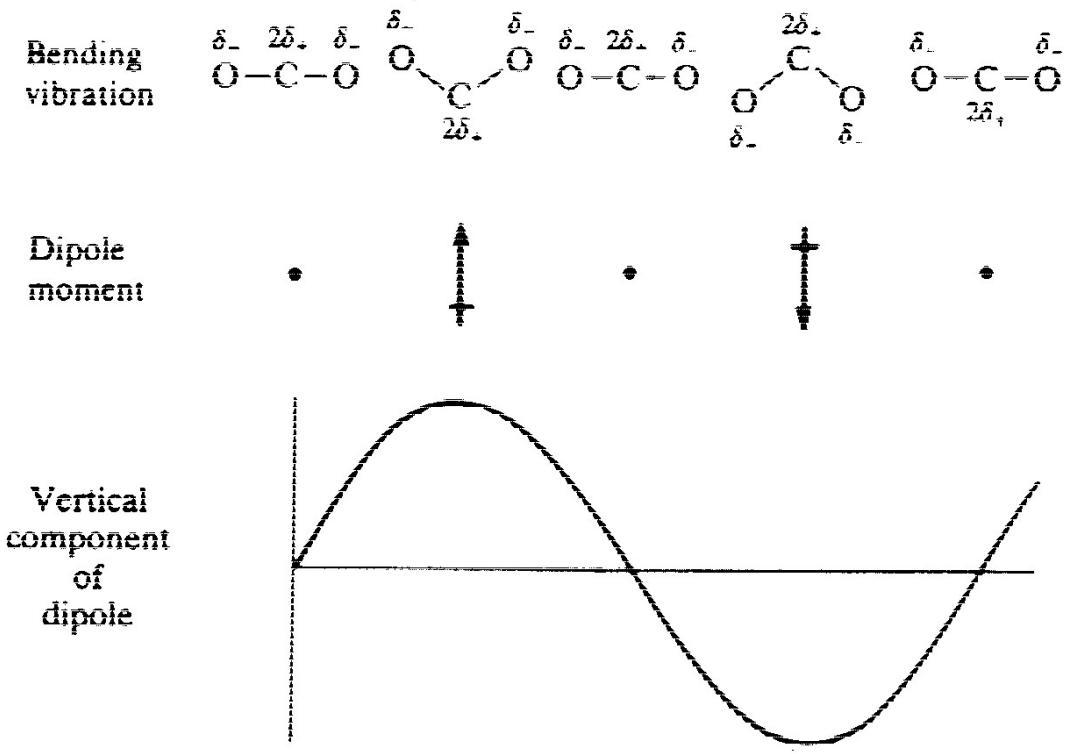

Transition dipole moment:

$\hat{\mu}' \neq 0$

IR active

Figure 1.8 The bending motion of the carbon dioxide molecule and its associated dipole fluctuation.

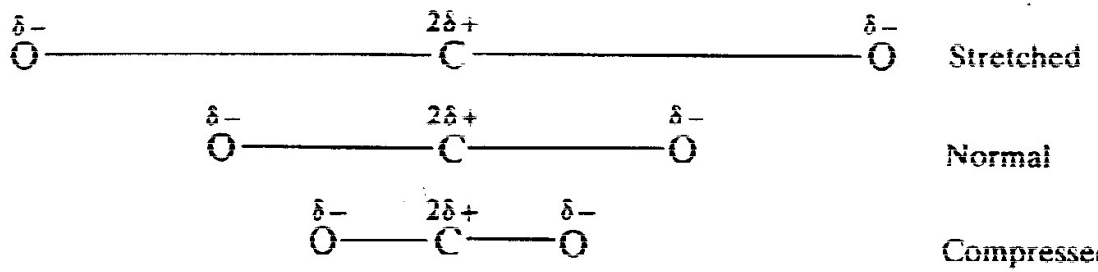

$\hat{\mu}' = 0$

IR inactive

Figure 1.6 The symmetric stretching vibration of the carbon dioxide molecule with amplitude much exaggerated.

Degrees of freedom

Stretching

In-plane bending

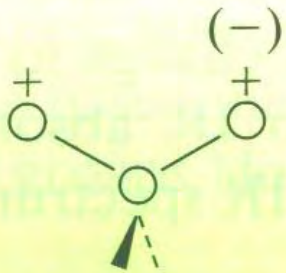

Out-of-plane bending

Total degrees of freedom in motion: translation, rotation, and *vibration*

Degrees of freedom in vibrations:

Linear molecules with N atoms:

3N-5 vibrational modes

Non-linear molecules with N atoms:

3N-6 vibrational modes

Motions of a free water molecule

Rotations

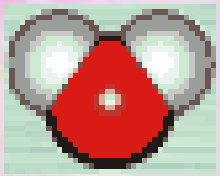

A = 27.8 cm^{-1}

B = 15.5 cm^{-1}

C = 9.95 cm^{-1}

Vibrations

3651.7 cm^{-1}

Infrared active

3755.8 cm^{-1}

Infrared active

1595.0 cm^{-1}

Infrared active

http://www.lsbu.ac.uk/water

Motions of water molecules in liquid water

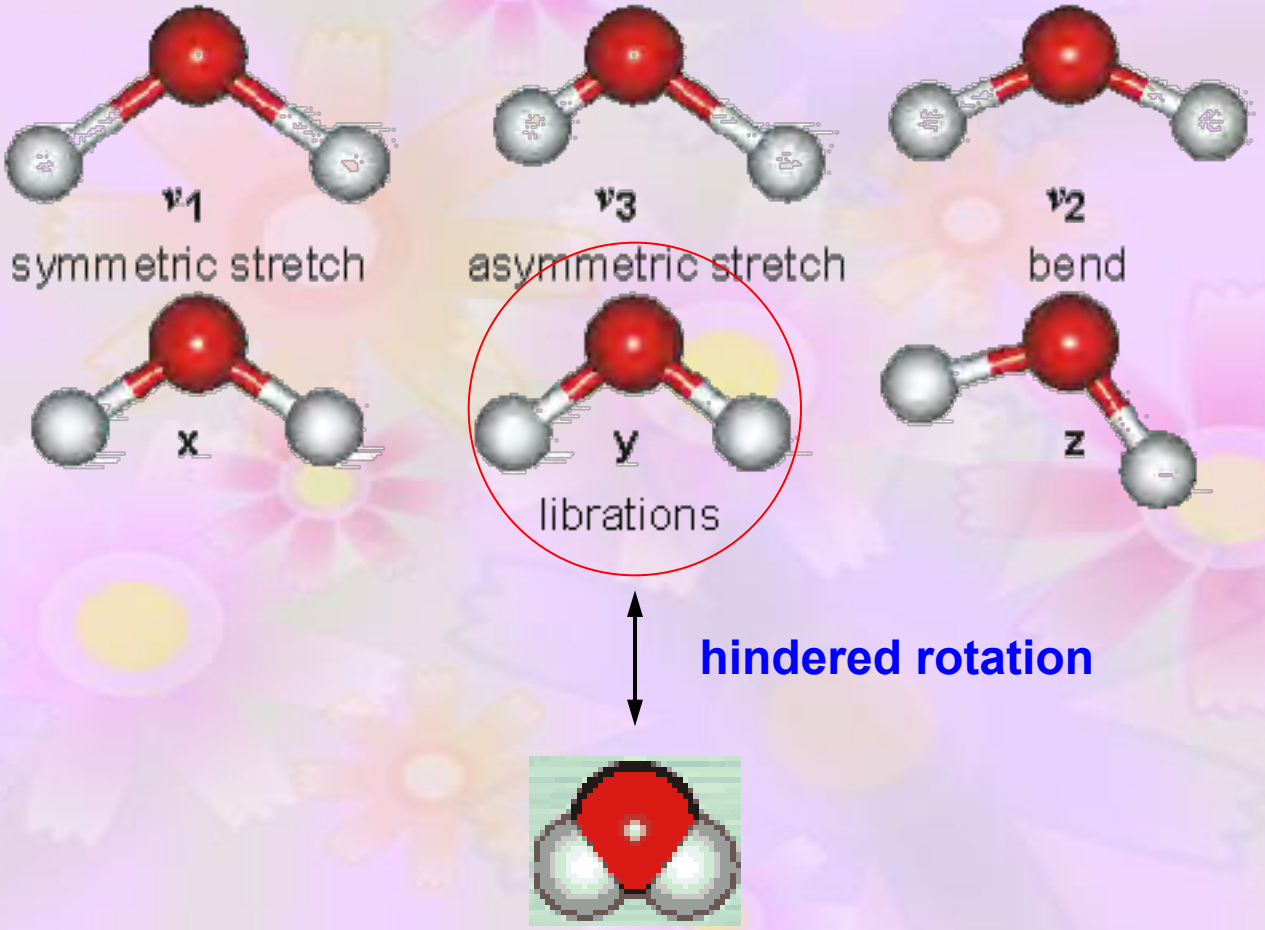

An example: 6 different vibrations of a CH_2 group

Symmetric stretching

Asymmetric stretching

Scissoring

Rocking

Wagging

Twisting

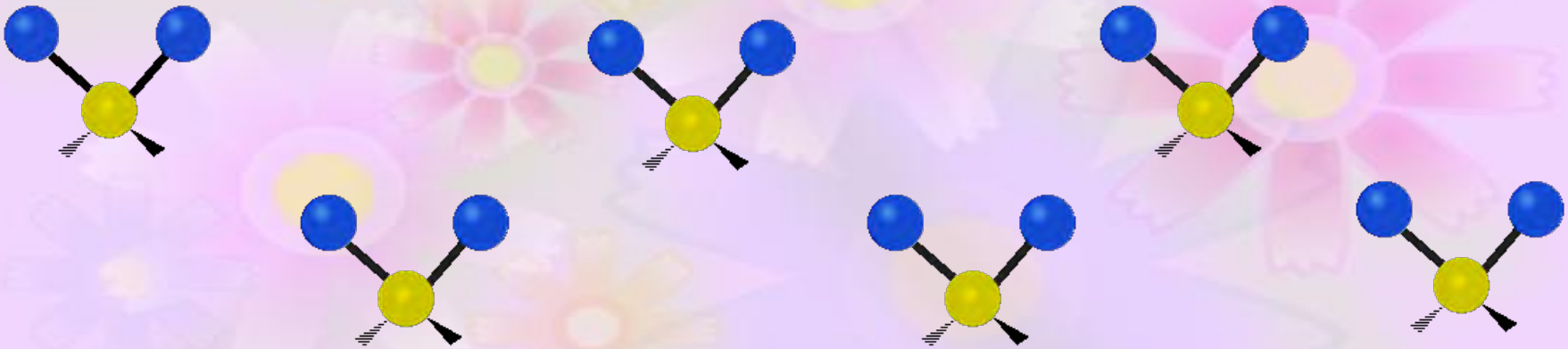

A typical RAIRS spectrometer

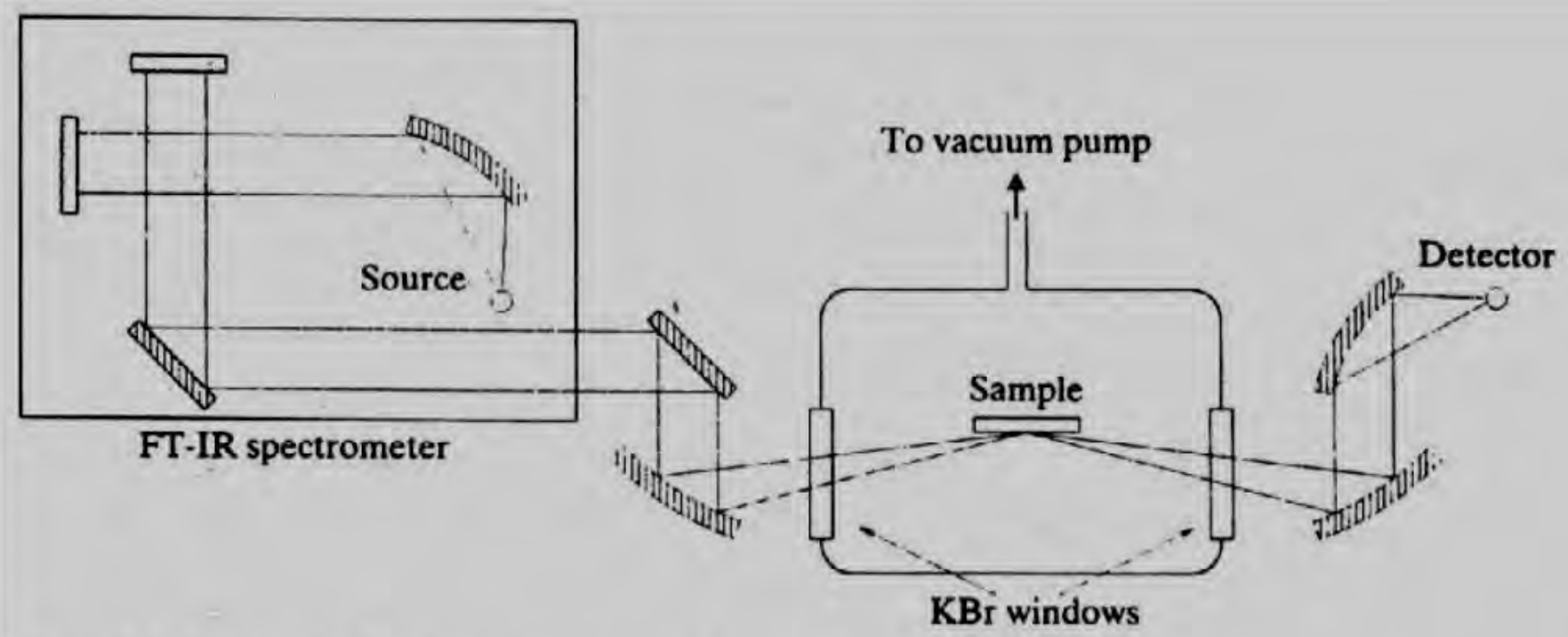

Figure 8.6 A typical reflection–absorption infra-red spectrometer (RAIRS).

IR spectra of C_2H_4 on Pt(111)

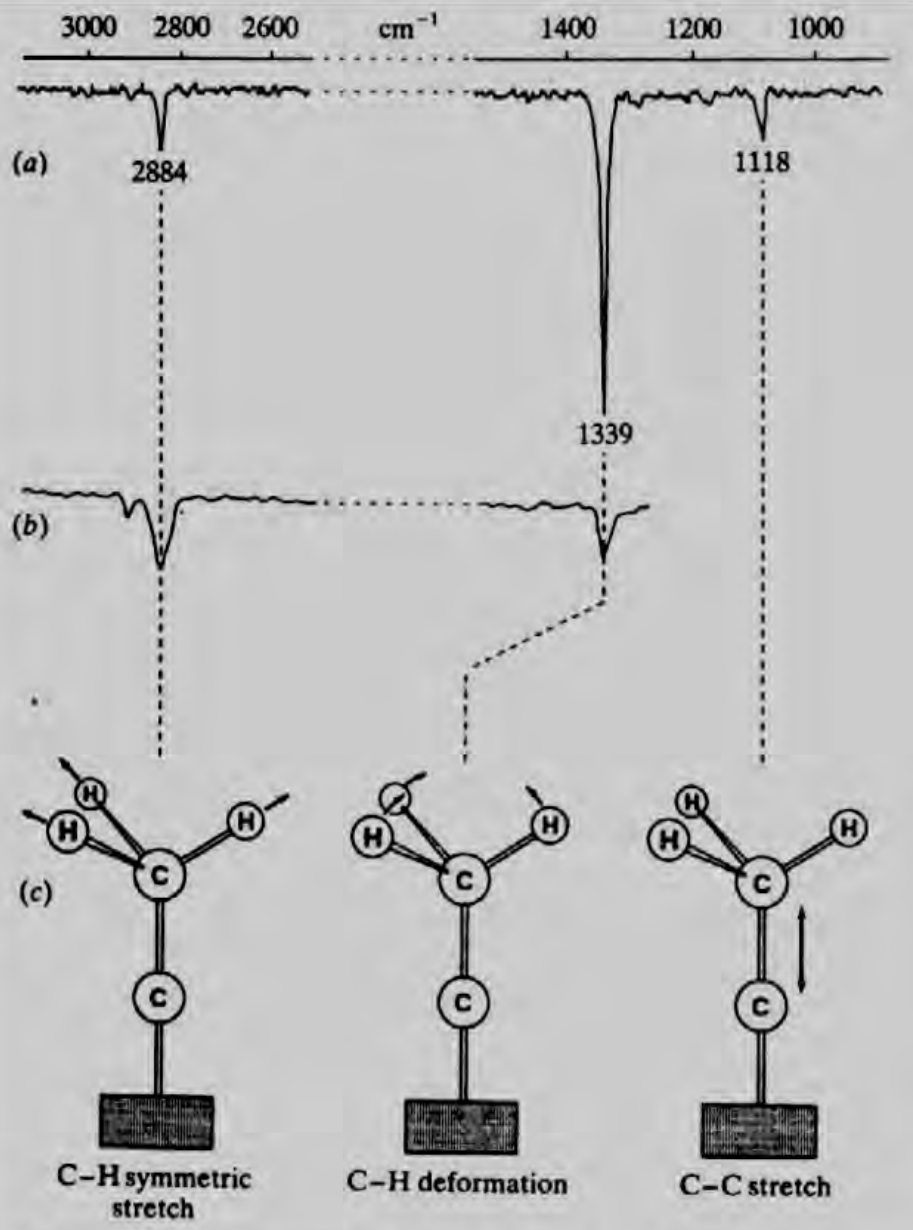

Table 8.1 Symmetric stretching frequencies for C—C and C—H bonds in ethyne, ethene, and ethane

	CC symmetric stretch (cm^{-1})	CH symmetric stretch (cm^{-1})
Ethyne, $HC{\equiv}CH$	1974	3374
Ethene, $H_2C{=}CH_2$	1620	3020
Ethane, $H_3C{-}CH_3$	990	2870

Figure 8.7 Infra-red spectra of ethene adsorbed on Pt surfaces: (*a*) RAIRS of ethylidyne on Pt(111), (*b*) transmission infra-red spectrum of ethene adsorbed on platinum supported on silica, and (*c*) the modes observed for ethylidyne. (*(a) and (b) reproduced with permission from M. A. Chesters, C. De la Cruz, P. Gardner, E. M. McCash, P. Pudney, G. Shahid and N. Sheppard,* J. Chem. Soc. Faraday Trans., **86***(15), 2757–2763, 1990.*)

Linear polarization spectroscopy

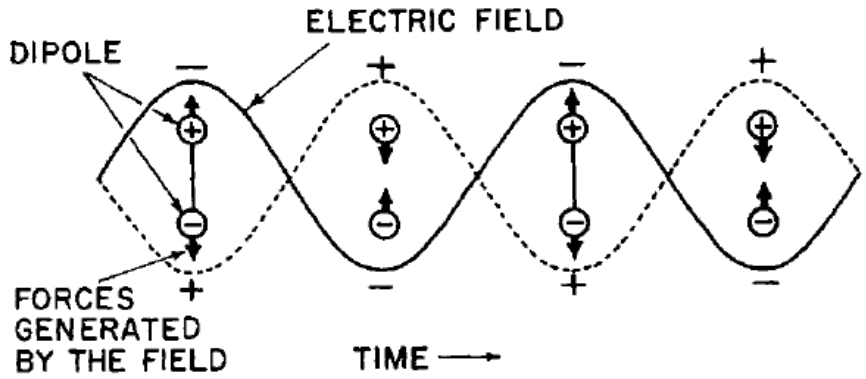

FIG. 1.6. Forces generated on a dipole by an oscillating electric field. These forces tend to alternately increase and decrease the dipole spacing.

$$H' = \mu \cdot E$$

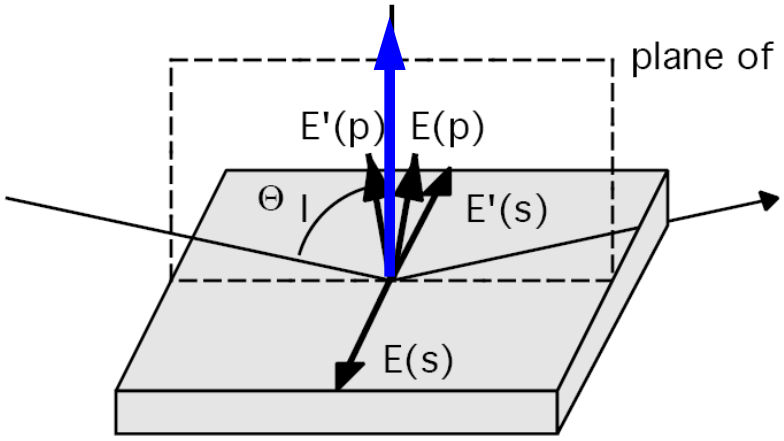

For a perpendicular dipole:

$H' = 0$ **for E(s)**

$H' \neq 0$ **for E(p)**

Orientation of SiH bonds on diamond surfaces

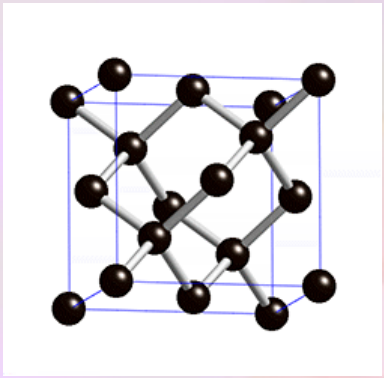

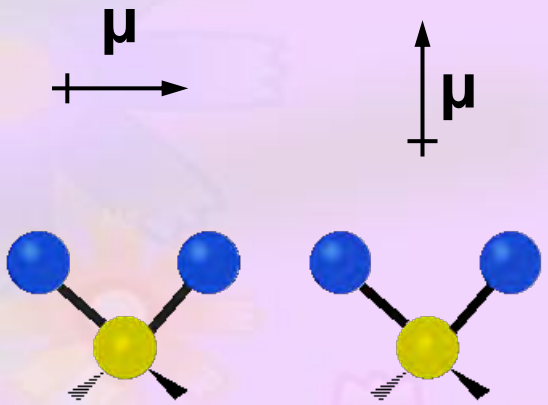

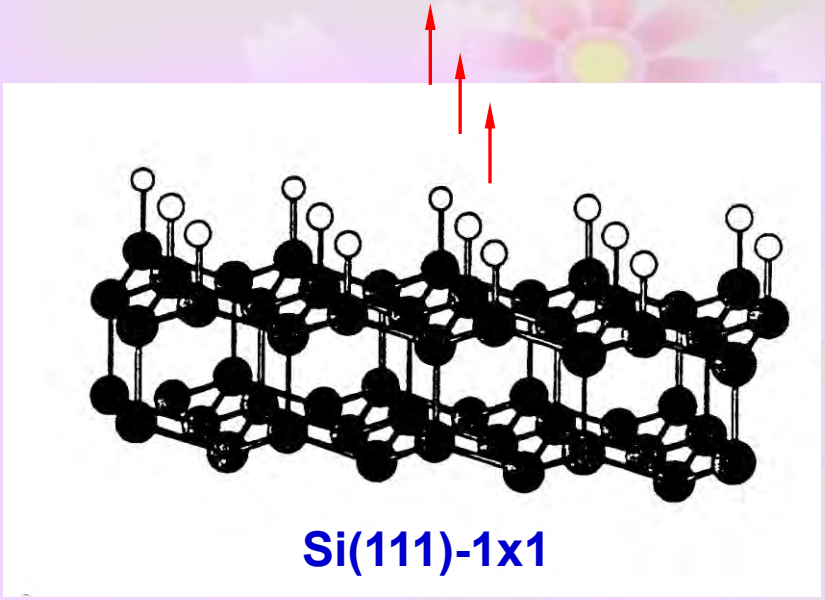

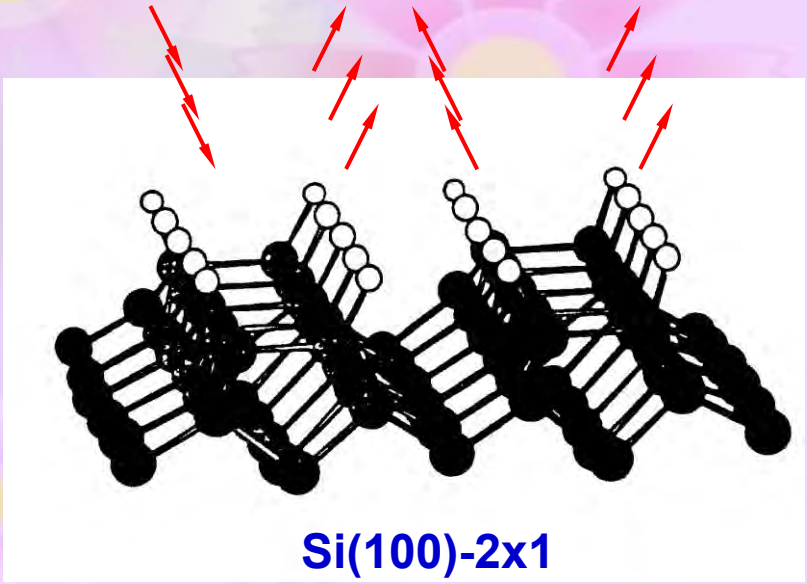

H on Si(111): An ideal H-terminated surface

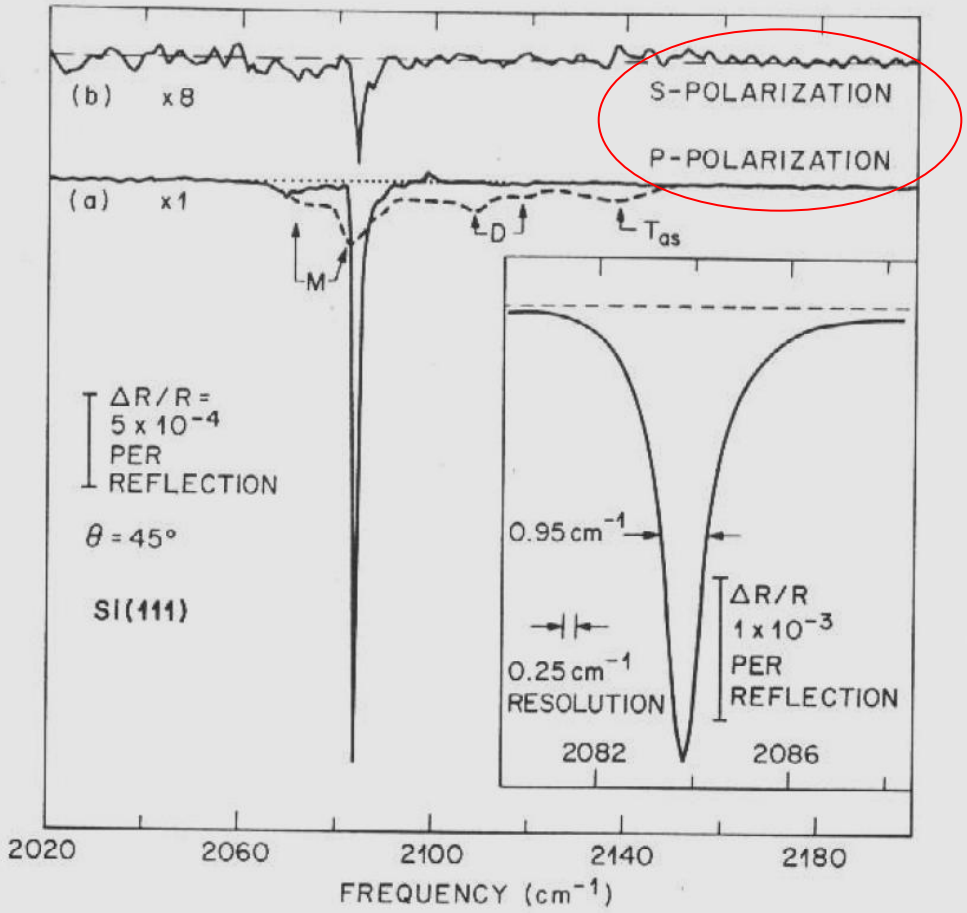

Figure 23 Internal reflection spectra of HF-treated Si(111) surfaces. (a) Surface treated with pH-modified buffered HF (pH 9–10)(solid curve) and with dilute HF (100:1 H_2O:HF)(dashed curve,) (b) s-polarization for surface treatment with pH-modified buffered HF (pH 9–10). Inset: High resolution spectrum of Si(111) surface treated with pH-modified buffered HF (pH 9–10). (From Ref. 60.)

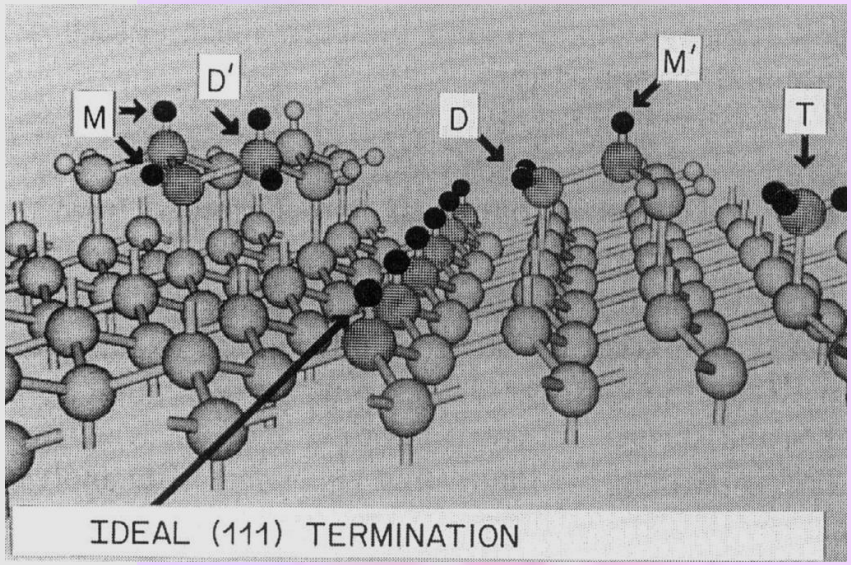

Higashi et al.
Appl. Phys. Lett. **56**, 656 (1990)

Helium atom scattering (HAS)

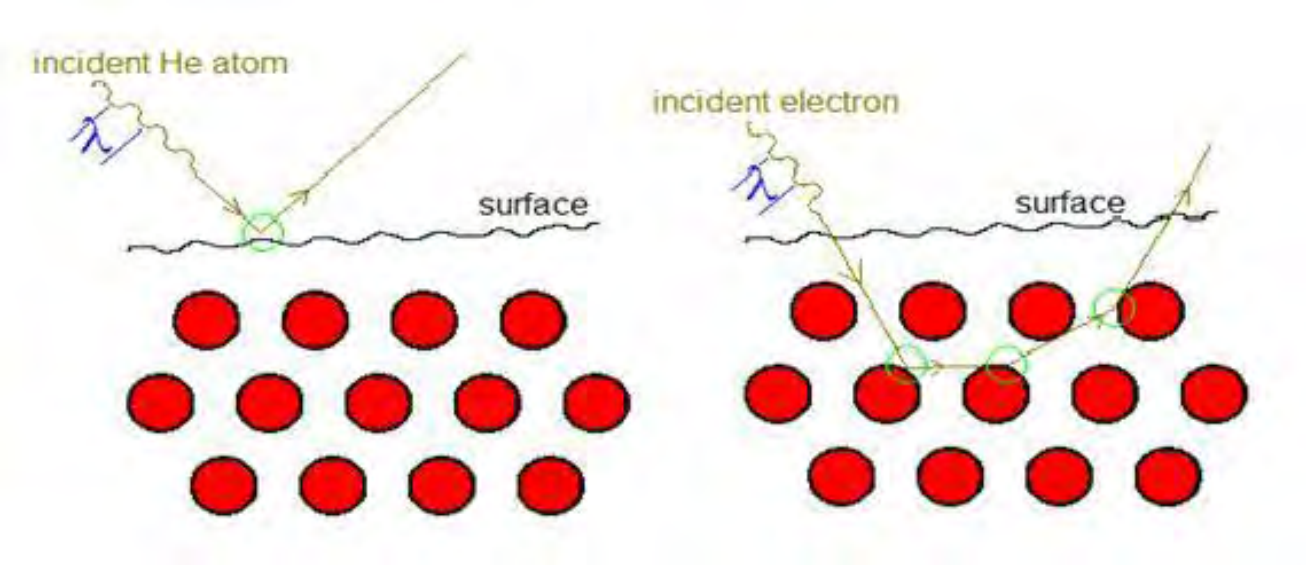

Advantages of using helium atoms as scattering agents:

•The lightweight helium atoms at thermal energies do not penetrate into the bulk of the material being studied and so is surface-sensitive.
•The de Broglie wavelength of helium atoms is on the order of the interatomic spacing of materials.
•Helium atoms are neutral and thus insensitive to surface charges.
•Helium atoms are chemically inert and non-destructive to the sample.

A typical HAS spectrometer

•The helium atom beam is created through free adiabatic expansion of helium at a pressure of ~200 bar into a low-vacuum chamber through a small (~5-10 μm) nozzle

•Typical helium atom energies produced are 5 – 200 meV, with a very narrow energy spread of less than 1 meV.

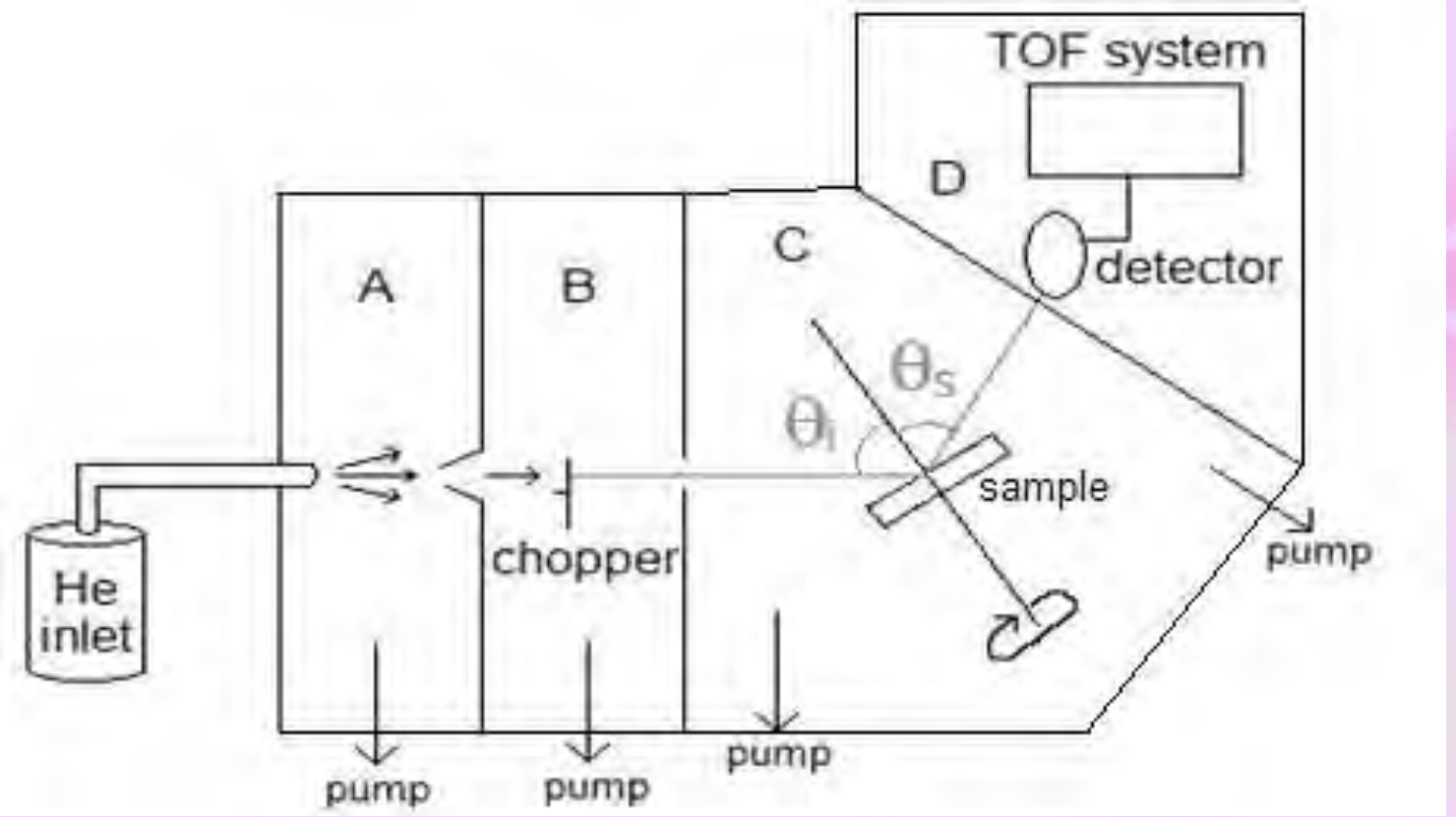

The Maxwell-Boltzmann distribution of molecular speeds

$$f(u) = 4\pi u^2 \left(\frac{m}{2\pi k_B T}\right)^{3/2} e^{-mu^2/2k_B T}$$

The distribution of speeds for nitrogen gas molecules at 3 different temperatures

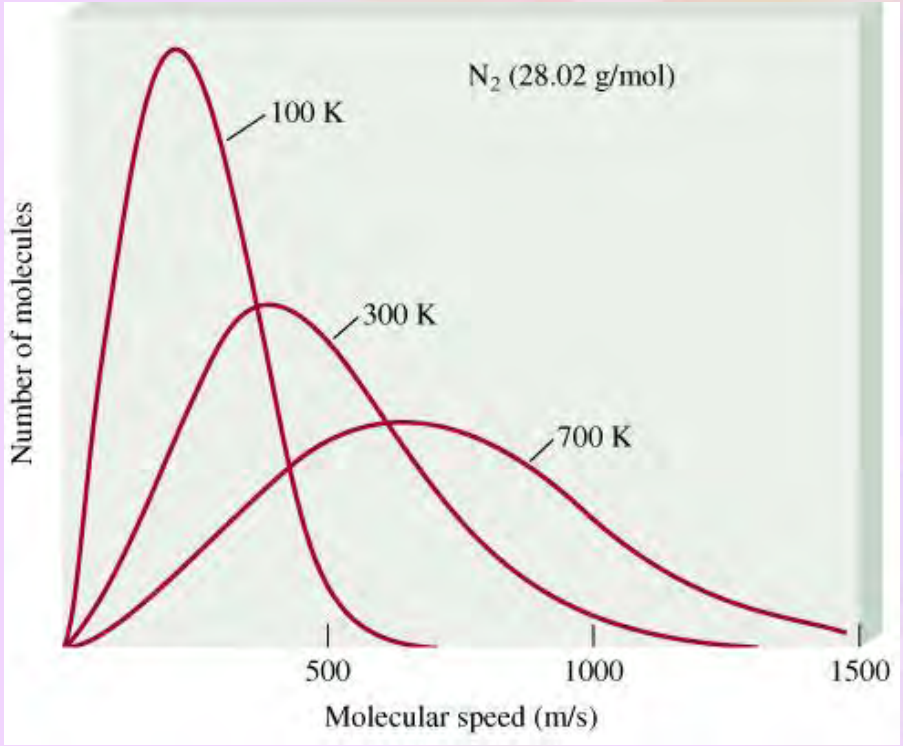

The distribution of speeds of 3 different gases at the same temperature

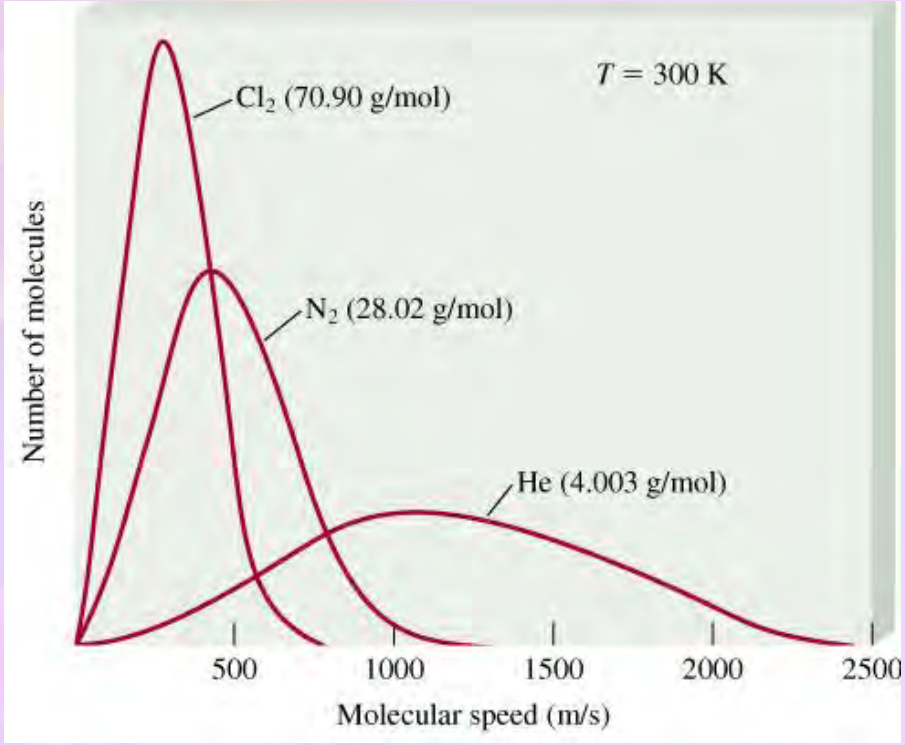

Apparatus for studying molecular speed distribution

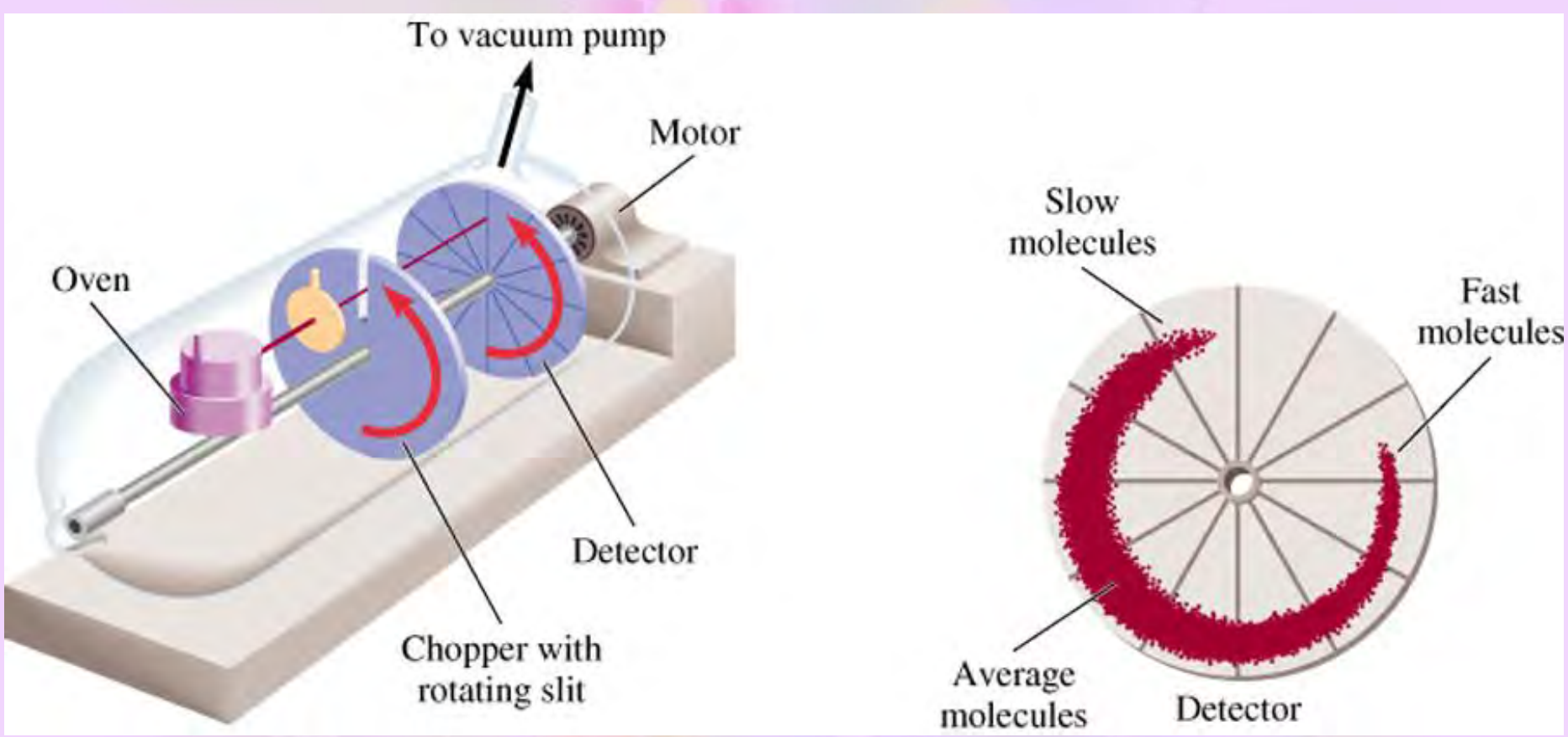

Hindered motions of adsorbate

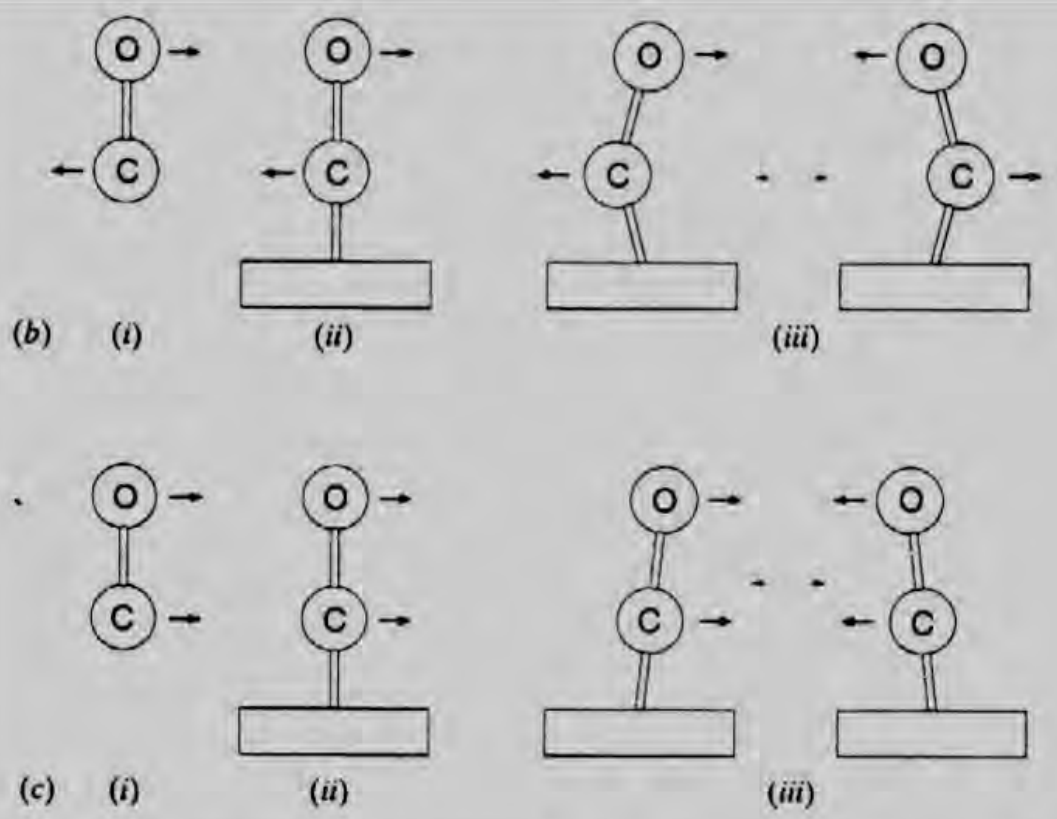

Inelastic He scattering

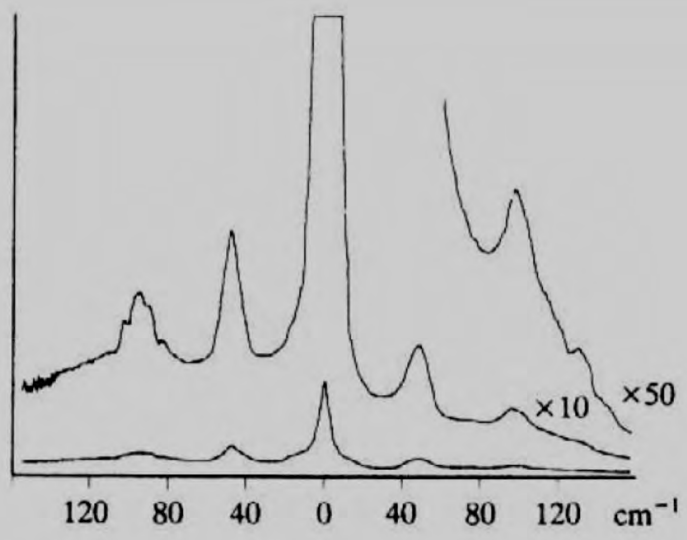

Figure 8.9 (*a*) Inelastic helium scattering for CO adsorbed on a Pt(111) surface at 300 K. The feature observed at 129 cm^{-1} is due to the hindered rotation which is illustrated in (*b*), while those at 48 and 96 cm^{-1} are due to the hindered translation mode shown in (*c*) and its first overtone. (*(a) is reproduced with permission from A. Lahee, P. Toennies and Ch.Wöll,* Surface Science, **177**, *371, 1986.*)

Degrees of freedom

Stretching

In-plane bending

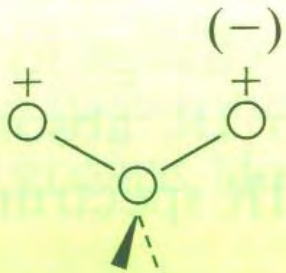

Out-of-plane bending

Total degrees of freedom in motion: translation, rotation, and *vibration*

Degrees of freedom in vibrations:

Linear molecules with N atoms:

3N-5 vibrational modes

Non-linear molecules with N atoms:

3N-6 vibrational modes

Electron energy loss spectroscopy (EELS)

High-resolution electron energy loss spectroscopy (HREELS)

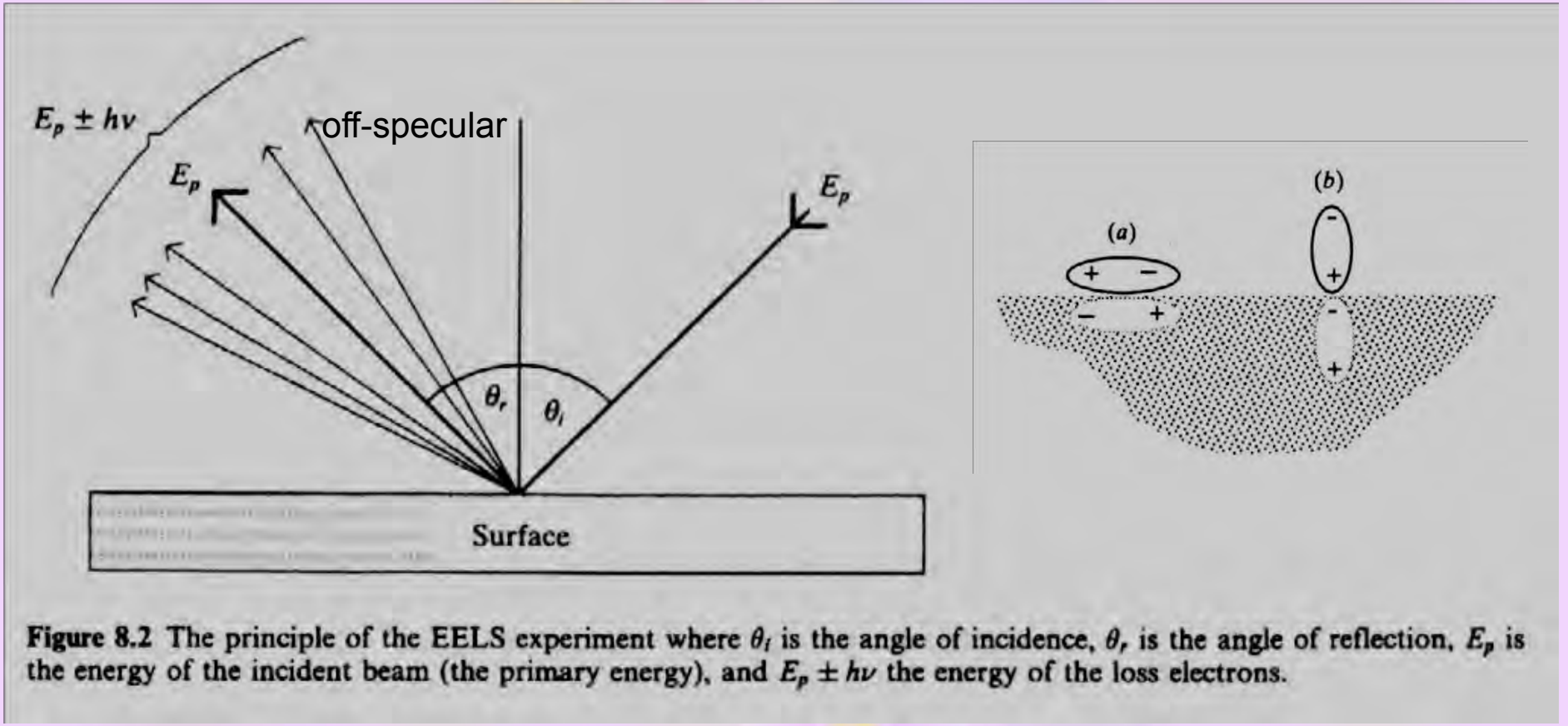

Figure 8.2 The principle of the EELS experiment where θ_i is the angle of incidence, θ_r is the angle of reflection, E_p is the energy of the incident beam (the primary energy), and $E_p \pm h\nu$ the energy of the loss electrons.

Banwell & McCash, *Fundamentals of Molecular Spectroscopy*, 4th Ed., Tata McGraw-Hill, 1994

A typical EEL spectrometer

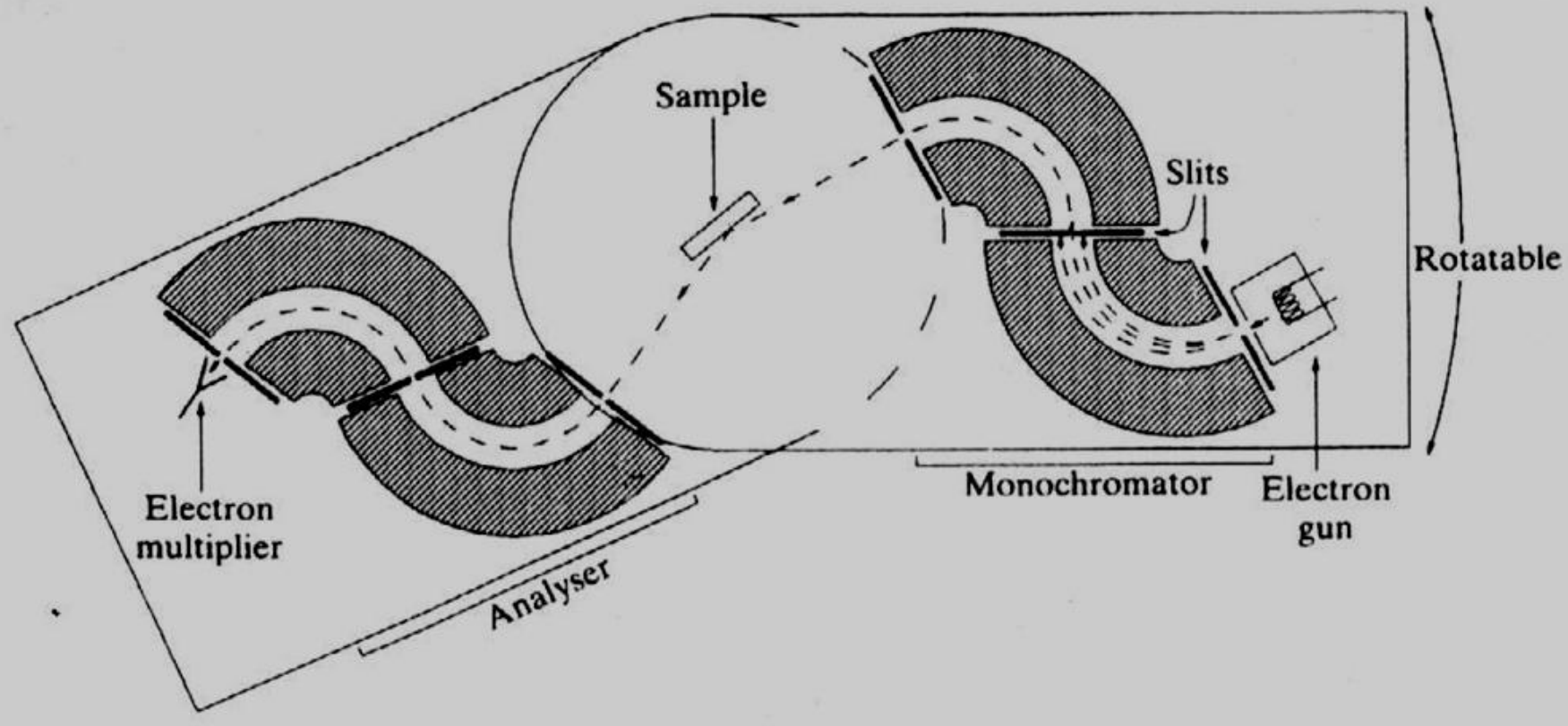

Figure 8.1 The electron energy loss spectrometer.

EEL spectra of C_2H_2 on Cu(111)

Table 8.1 Symmetric stretching frequencies for C—C and C—H bonds in ethyne, ethene, and ethane

	CC symmetric stretch (cm^{-1})	CH symmetric stretch (cm^{-1})
Ethyne, $HC{\equiv}CH$	1974	3374
Ethene, $H_2C{=}CH_2$	1620	3020
Ethane, $H_3C{-}CH_3$	990	2870

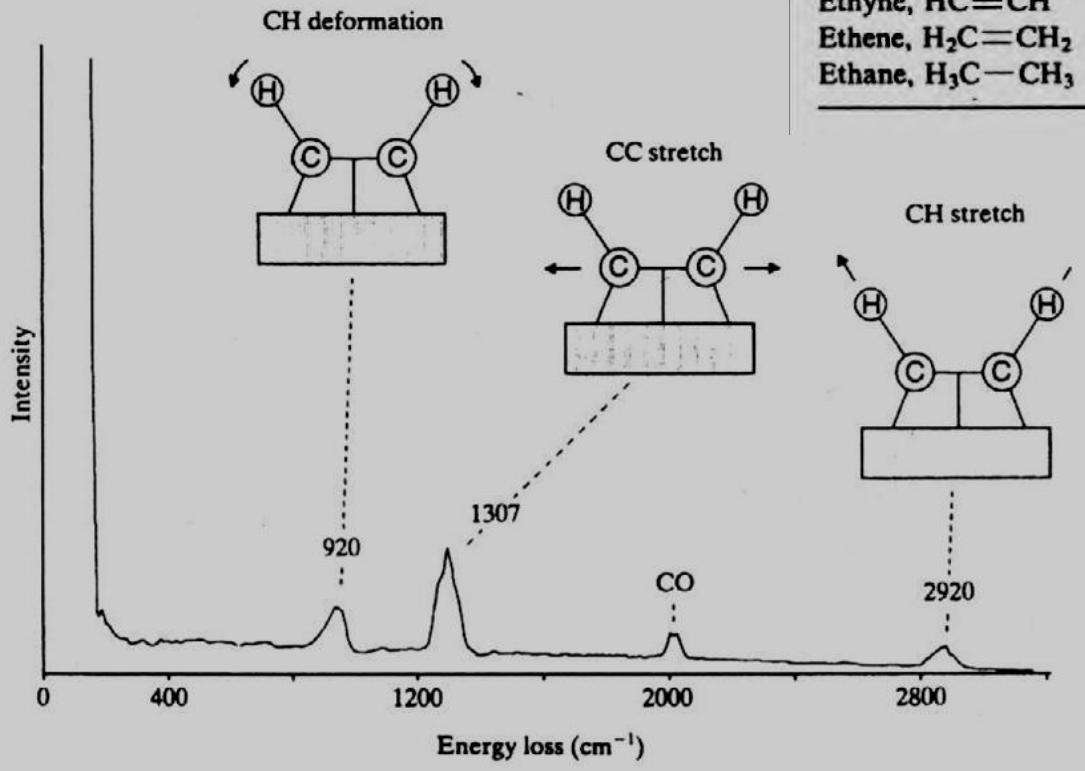

Figure 8.4 Electron energy loss spectrum of ethyne adsorbed on the Cu(111) surface. (*Reproduced with permission from B. J. Bandy, M. A. Chesters, M. E. Pemble, G. S. MacDougall and N. Sheppard,* Surface Science, **139**, *87, 1984.*)

1 eV = 8064 cm^{-1}

IR versus EEL spectra

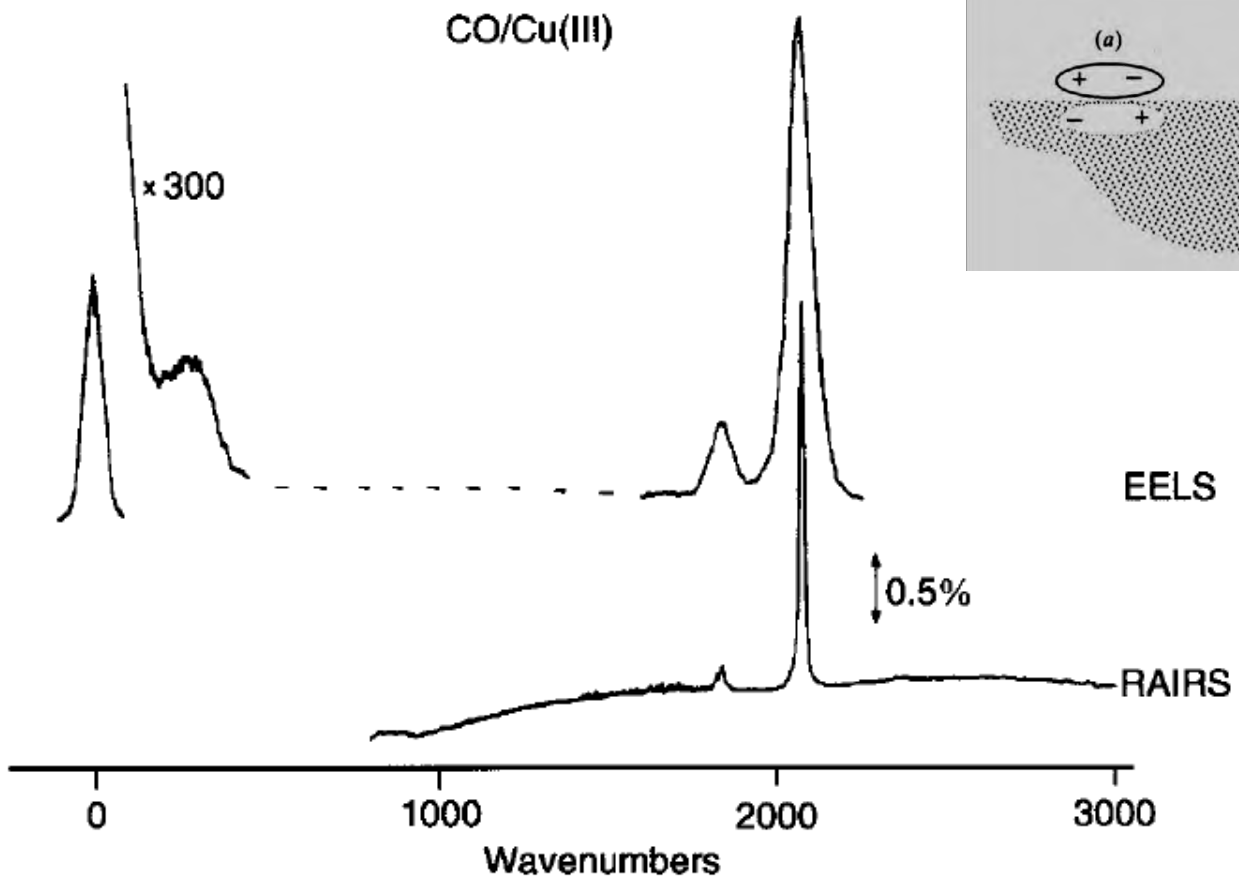

Figure 7.13. RAIRS spectrum of a monlayer of CO adsorbed on a Cu (111) surface at 95 K in comparison with analogous data obtained using electron energy loss spectroscopy, after Chesters *et al.* [10]

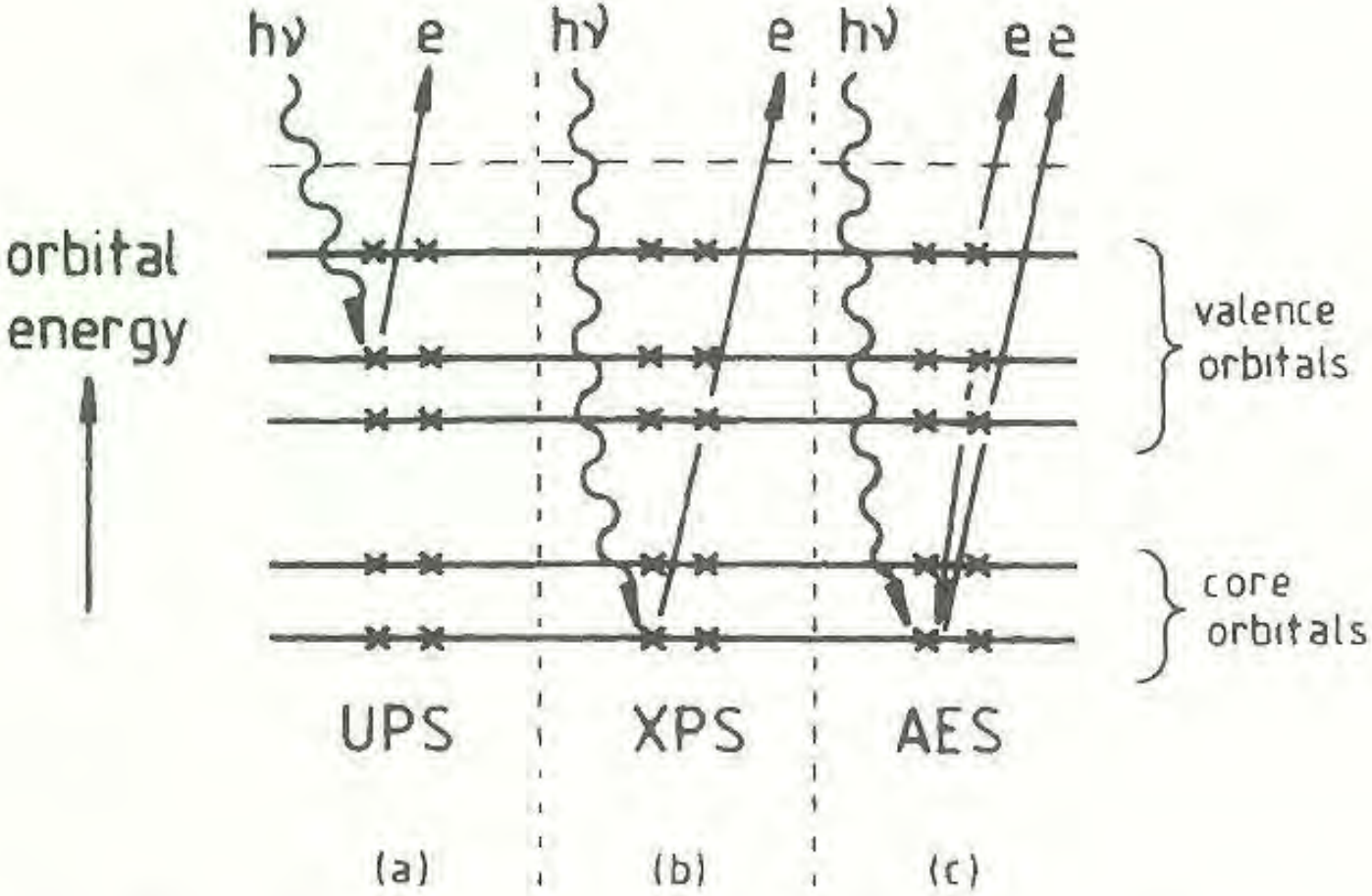

Figure 8.1 Processes occurring in (a) ultraviolet photoelectron spectroscopy (UPS), (b) X-ray photoelectron spectroscopy (XPS), (c) Auger electron spectroscopy (AES)

Photoelectron spectroscopy (PES)

Photoelectron spectroscopy involves the ejection of electrons from atoms or molecules following bombardment by monochromatic photons. The ejected electrons are called photoelectrons and were mentioned, in the context of the photoelectric effect, in Section 1.2. The effect was observed originally on surfaces of easily ionizable metals, such as the alkali metals. Bombardment of the surface with photons of tunable frequency does not produce any photoelectrons until the threshold frequency is reached (see Figure 1.2). At this frequency, ν_t, the photon energy is just sufficient to overcome the work function Φ of the metal, so that

$$h\nu_t = \Phi \tag{8.1}$$

At higher frequencies the excess energy of the photons is converted into kinetic energy of the photoelectrons

$$h\nu = \Phi + \tfrac{1}{2} m_e v^2 \tag{8.2}$$

where m_e and v are their mass and velocity.

Work functions of alkali metal surfaces are only a few electronvolts† so that the energy of near ultraviolet radiation is sufficient to produce ionization.

Photoelectron spectroscopy is a simple extension of the photoelectric effect involving the use of higher energy incident photons and applied to the study not only of solid surfaces but also of samples in the gas phase. Equations (8.1) and (8.2) still apply but, for gas phase measurements in particular, the work function is usually replaced by the ionization energy I‡, so that equation (8.2) becomes

$$h\nu = I + \tfrac{1}{2} m_e v^2 \tag{8.3}$$

$h\nu = E_{KE} + BE$ (binding energy)

A typical PES spectrometer

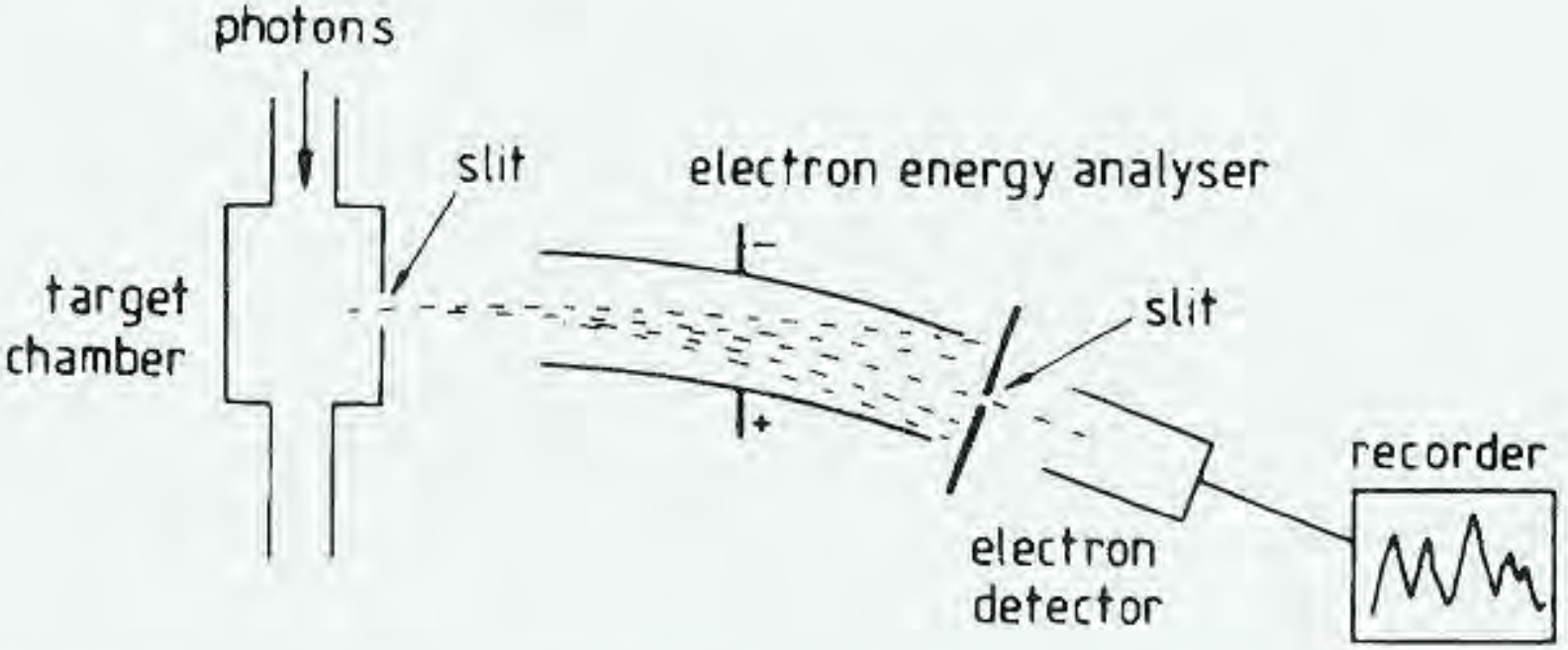

Figure 8.2 The principal components of a photoelectron spectrometer

UV photoelectron spectrum of CO

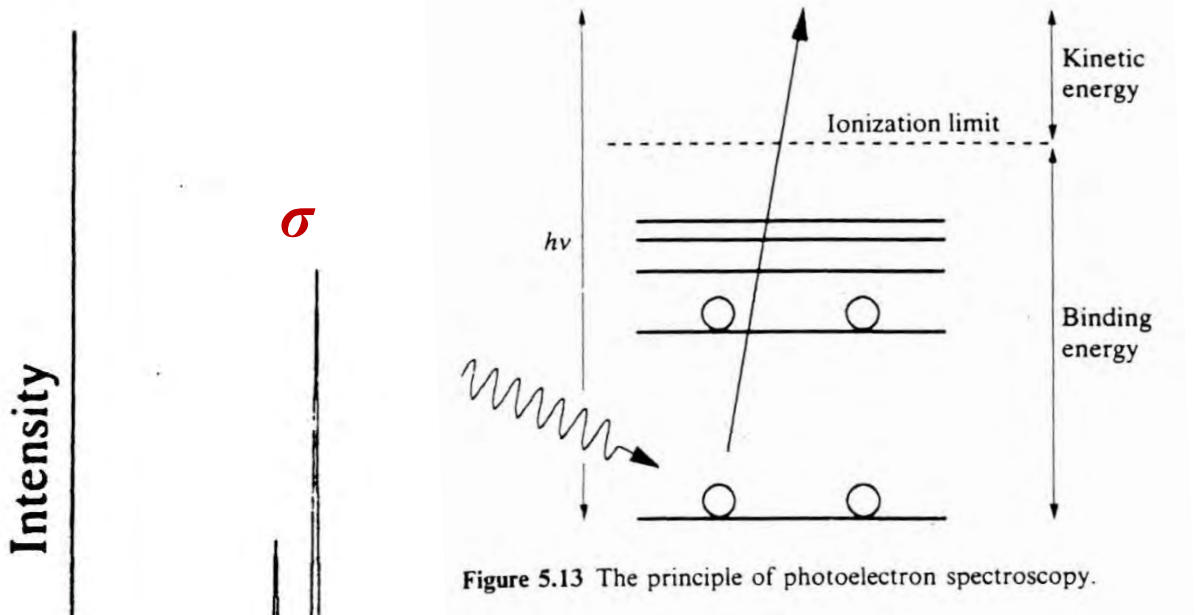

Figure 5.13 The principle of photoelectron spectroscopy.

Figure 6.21 The photoelectron spectrum of carbon monoxide.

X-ray photoelectron spectra

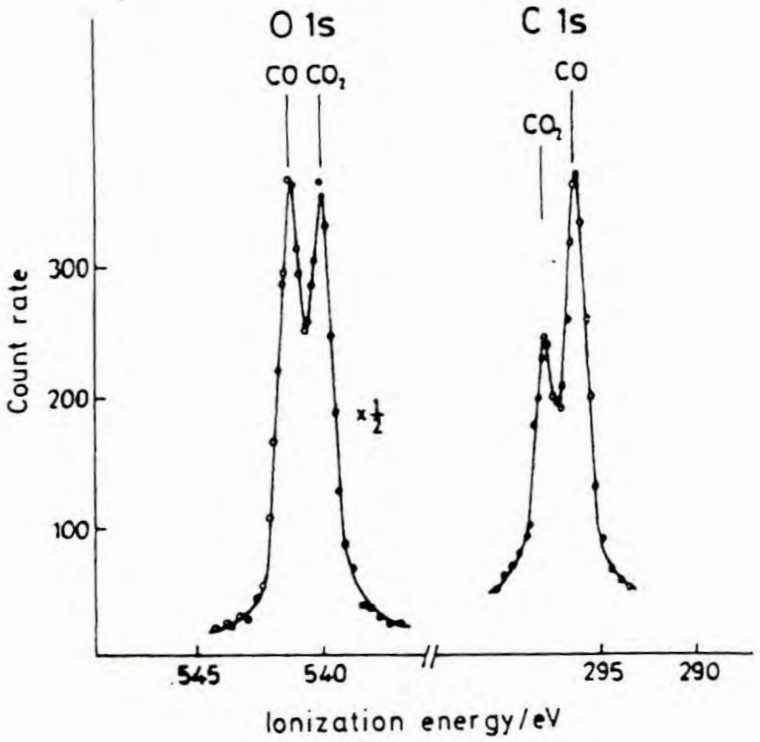

Figure 8.13 The Mg$K\alpha$ oxygen 1s and carbon 1s XPS spectra of a 2 : 1 mixture of CO and CO_2 gases. (Reproduced, with permission, from Allan, C. J., and Siegbahn, K. (November 1971), *Publication No. UUIP–754*, p. 48, Uppsala University Institute of Physics)

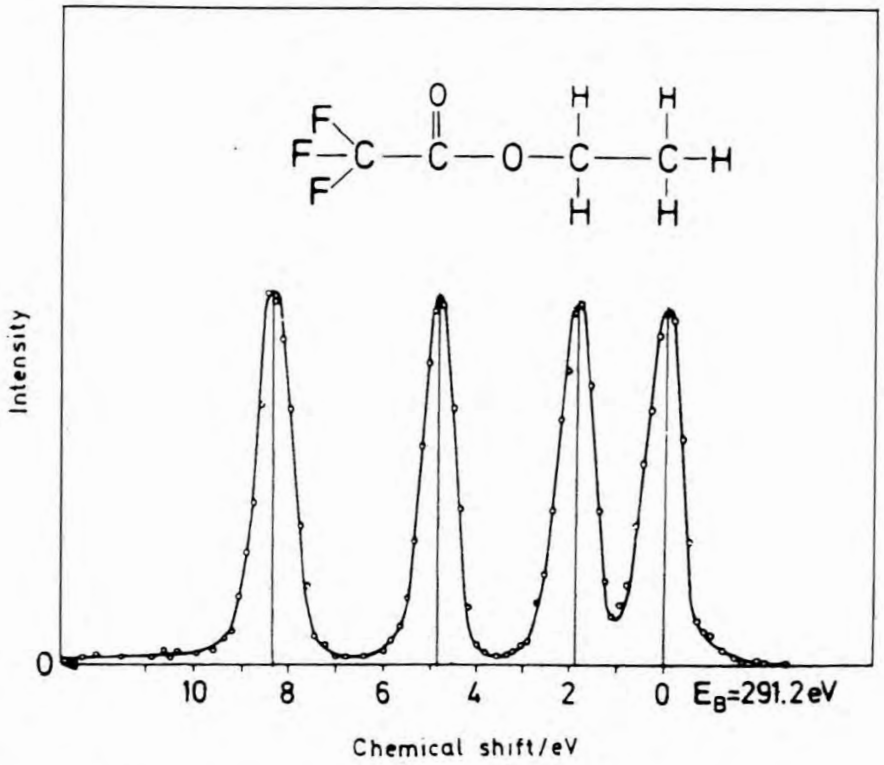

Figure 8.14 The monochromatized Al$K\alpha$ carbon 1s XPS spectrum of ethyltrifluoroacetate showing the chemical shifts relative to an ionization energy of 291.2 eV. (Reproduced, with permission, from Gelius, U., Basilier, E., Svensson, S., Bergmark, T., and Siegbahn, K., *J. Electron Spectrosc.*, **2**, 405, 1974)

Analysis of Electron Spectra of Carbon Allotropes (Diamond, Graphite, Fullerene) by Density Functional Theory Calculations Using the Model Molecules

K. Endo,*,† S. Koizumi,† T. Otsuka,† T. Ida,† T. Morohashi,‡ J. Onoe,§ A. Nakao,§ E. Z. Kurmaev,|| A. Moewes,⊥ and D. P. Chong#

Department of Chemistry, Faculty of Science, Kanazawa University, Kanazawa 920-1192 Japan, Analytical Laboratory, Ulvac-PHI, Chigasaki 253-0084 Japan, The Institute of Physical and Chemical Research, Wako, Saitama 351-01 Japan, Institute of Metal Physics, Russian Academy of Sciences-Ural Division 620219, Yekaterinburg GSP-170 Russia, Department of Physics and Engineering Physics, University of Saskatchewan, 116 Science Place, Saskatoon, SK, Canada S7N 5E2, and Department of Chemistry, 2036 Main Mall, University of British Columbia, Vancouver, BC, Canada V6T 1Z1

Received: March 5, 2003; In Final Form: June 23, 2003

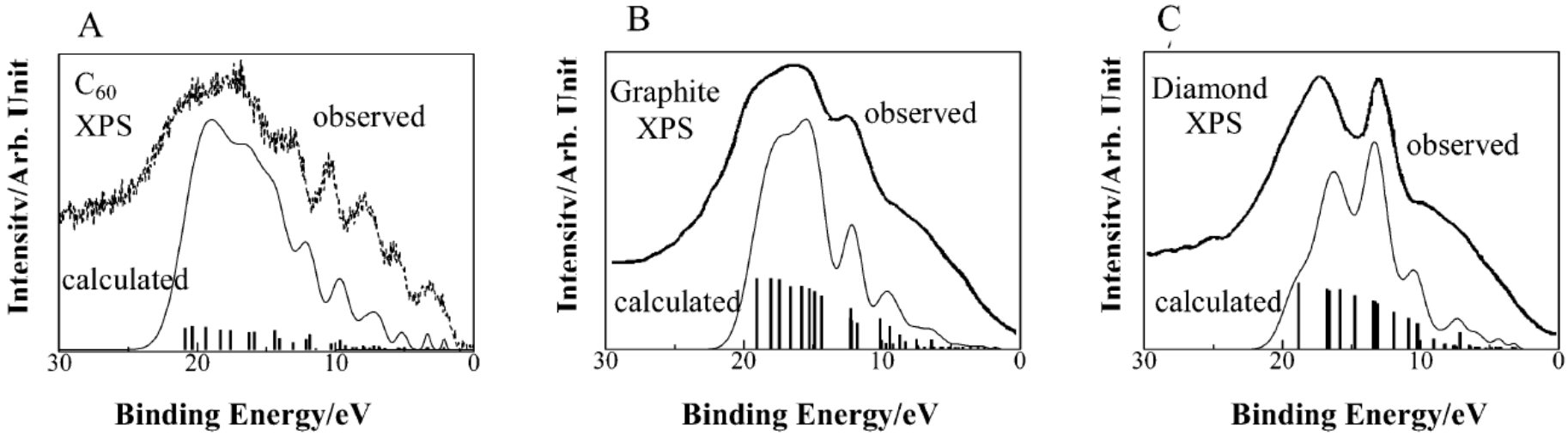

Auger electron spectroscopy (AES)

$$E_{Auger} + E_z = E_x - E_y \quad \text{or} \quad E_{Auger} = E_x - E_y - E_z$$

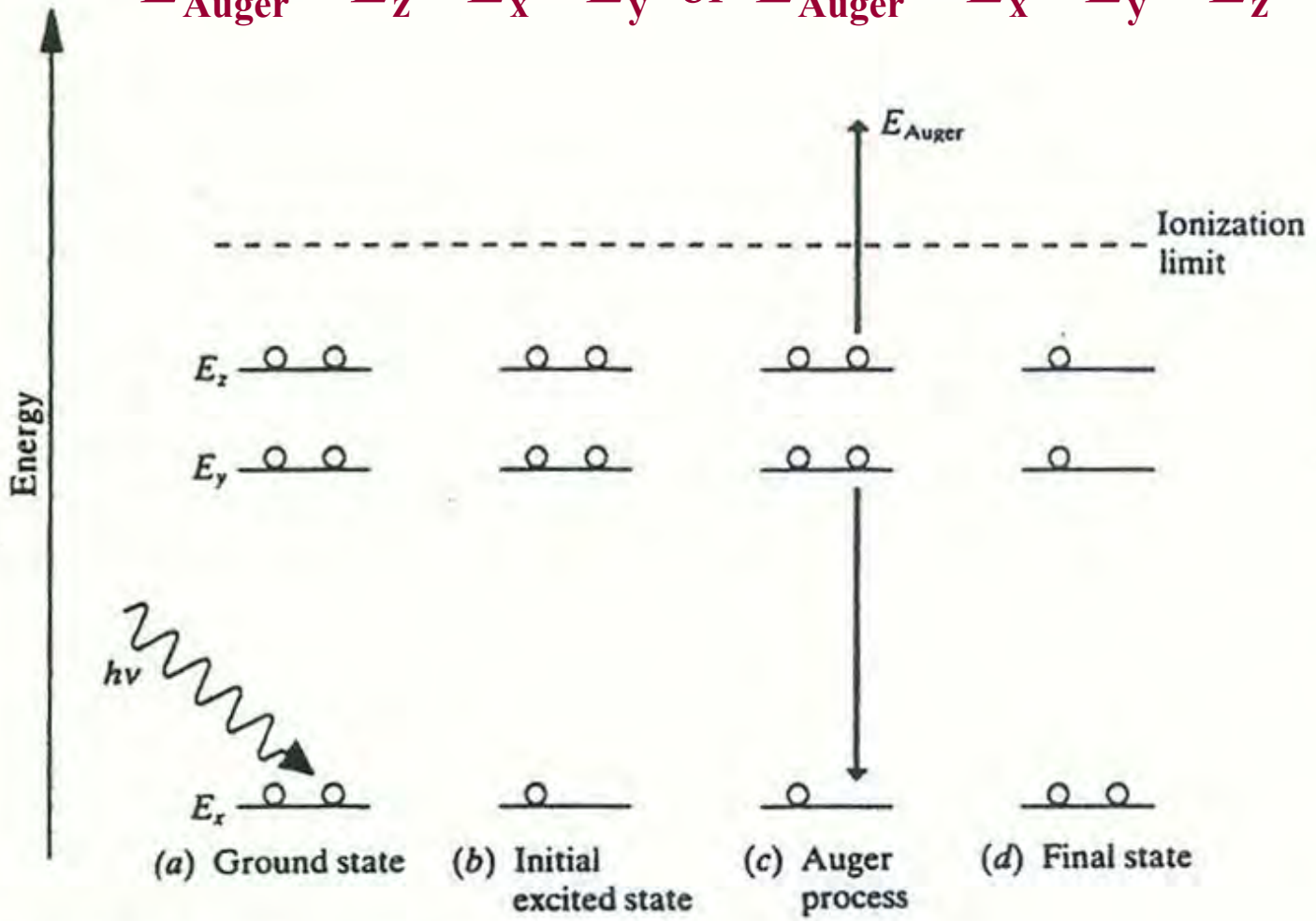

Figure 8.11 The Auger process.

Typical Auger electron spectra

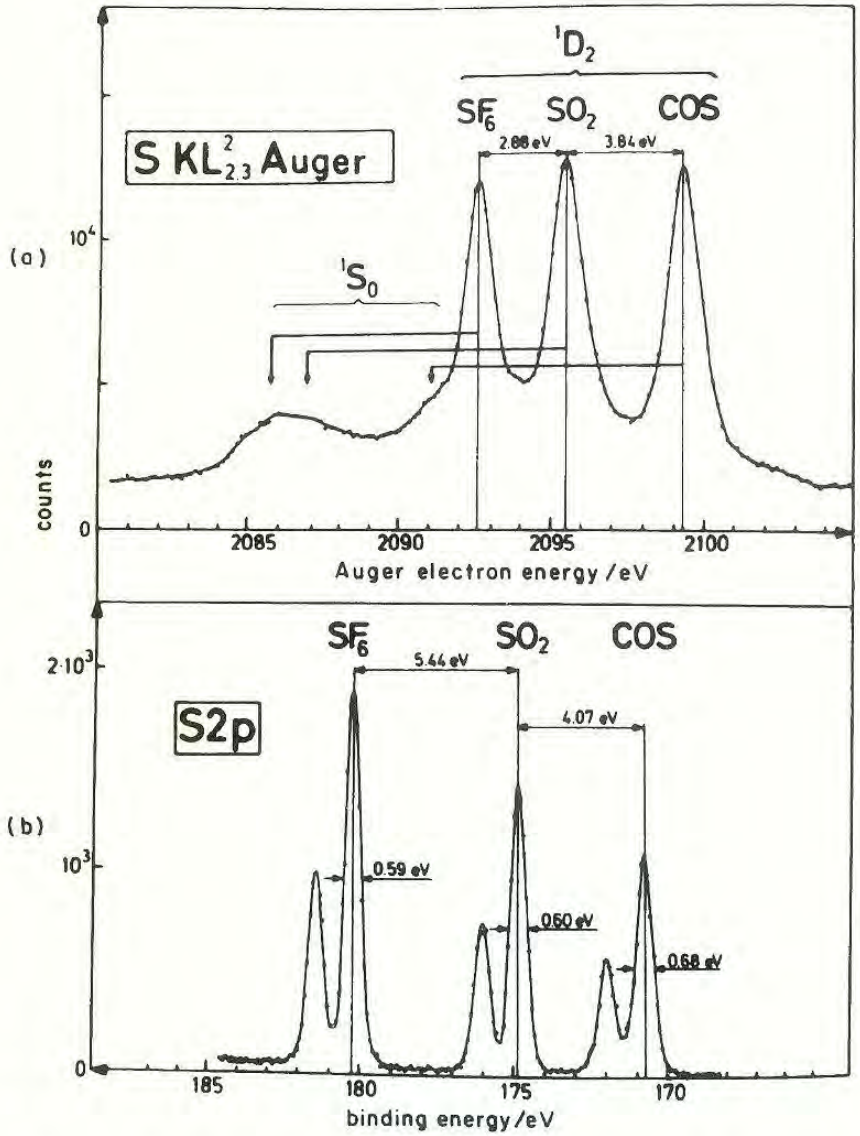

Figure 8.25 (a) The $KL_{II,III}L_{II,III}$ ($^1D_2$ and $^1S_0$) Auger spectrum of sulphur in a gaseous mixture of SF_6, SO_2, and OCS, compared with (b) the S 2*p* X-ray photoelectron spectrum of a mixture of the same gases. (Reproduced, with permission, from Aslund, L., Kelfve, P., Siegbahn, H., Goscinski, O., Fellner-Feldegg, H., Hamrin, K., Blomster, B., and Siegbahn, K., *Chem. Phys. Letters*, **40**, 353, 1976)

Diamond growth by chemical vapor deposition (CVD)

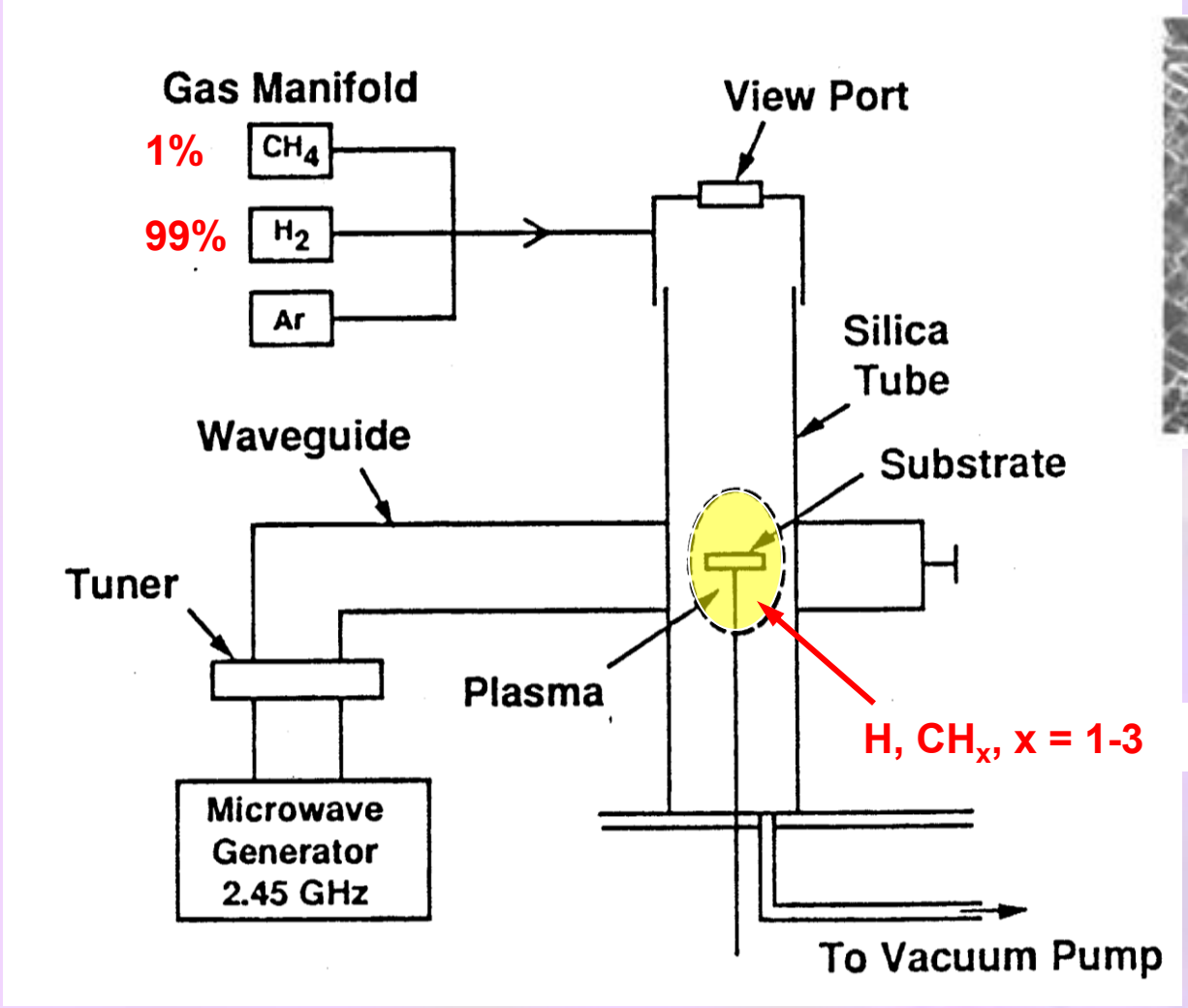

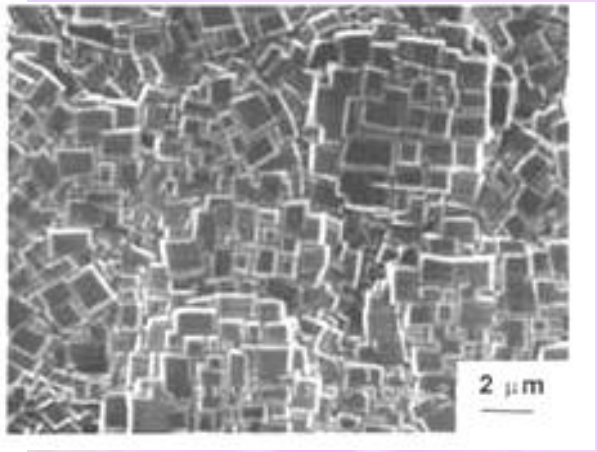

C(100)

Figure 1. Auger spectra of natural diamonds (A to C), CVD diamonds (D to G), HOPG (H) and glassy carbon (I). A_0 is the main peak and A_1 is the satellite peak which shows the significant difference between sp^3- and sp^2-bound carbons.

HOPG: highly oriented pyrolytic graphite

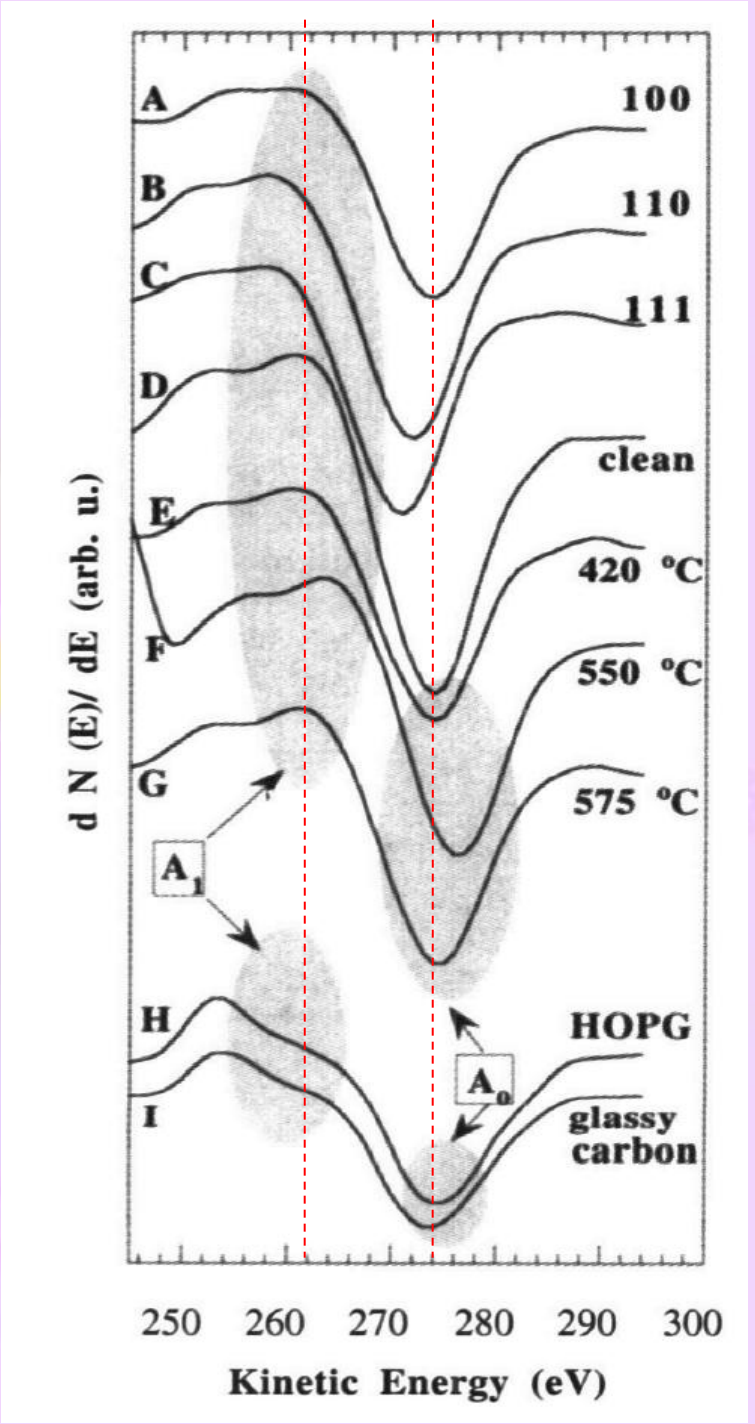

H on Si(111): An ideal H-terminated surface

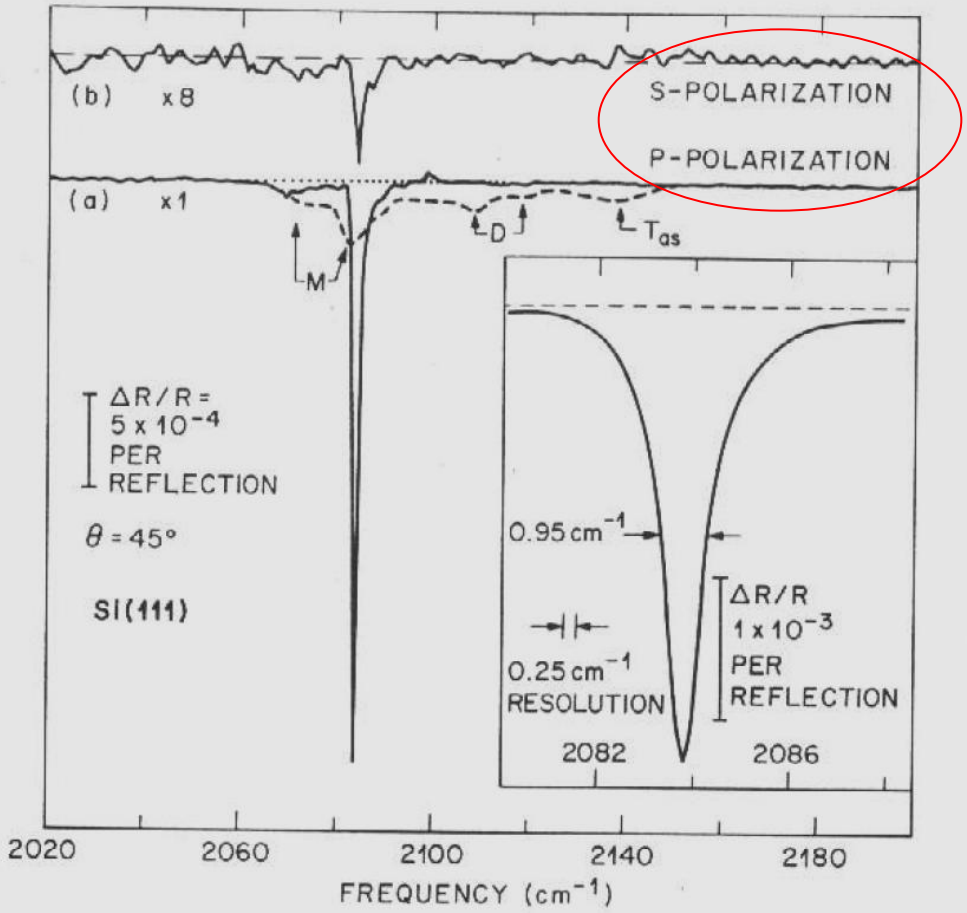

Figure 23 Internal reflection spectra of HF-treated Si(111) surfaces. (a) Surface treated with pH-modified buffered HF (pH 9–10)(solid curve) and with dilute HF (100:1 H_2O:HF)(dashed curve,) (b) s-polarization for surface treatment with pH-modified buffered HF (pH 9–10). Inset: High resolution spectrum of Si(111) surface treated with pH-modified buffered HF (pH 9–10). (From Ref. 60.)

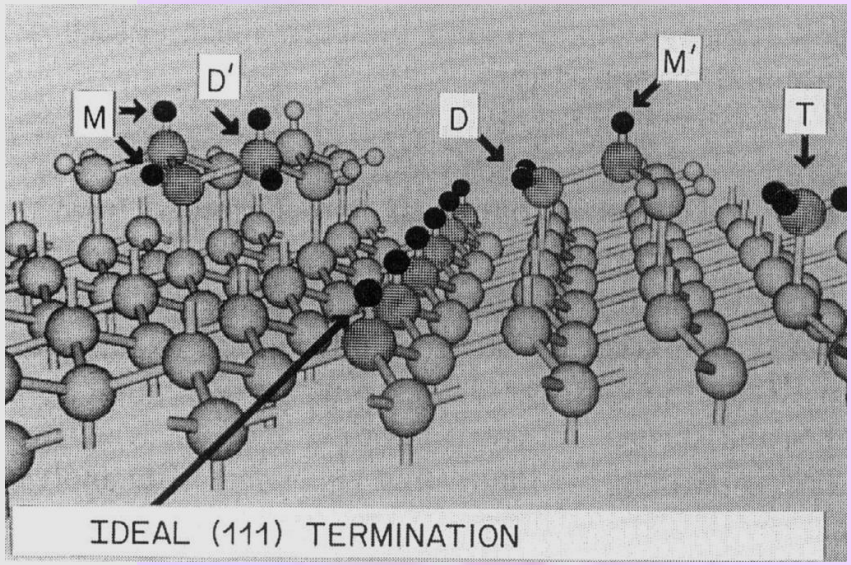

Higashi et al.
Appl. Phys. Lett. **56**, 656 (1990)

Attenuated total reflection (ATR) spectroscopy

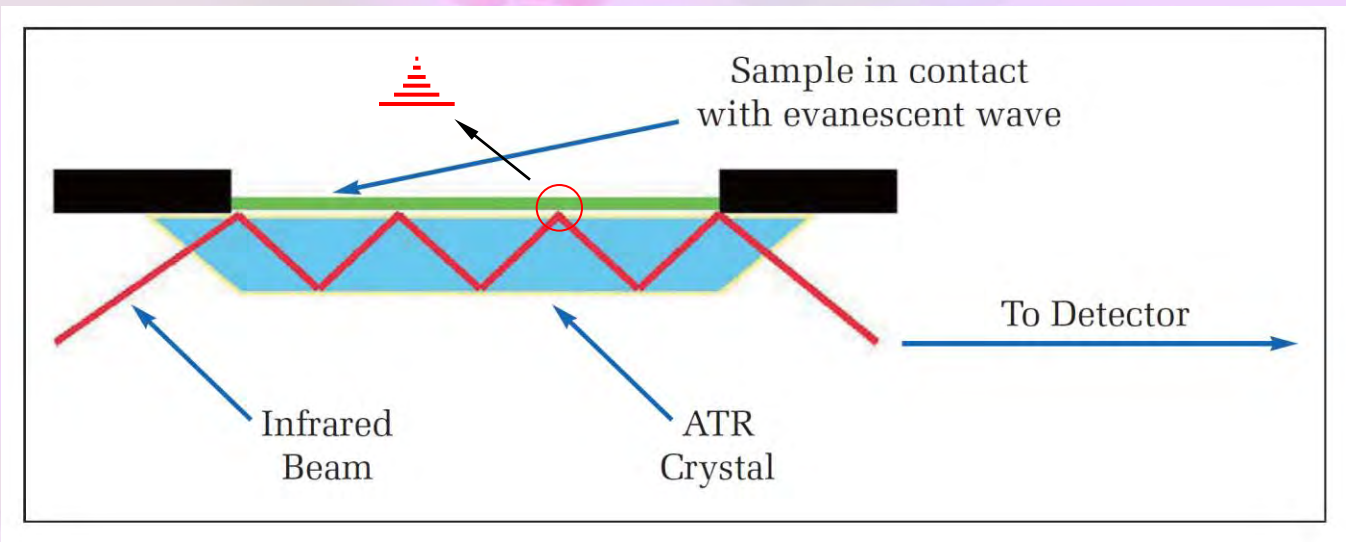

"Evanescent" means "tending to vanish", which is appropriate because the intensity of evanescent waves decays exponentially (rather than sinusoidally) with distance from the interface at which they are formed.

Evanescent waves are formed when sinusoidal waves are (internally) reflected off an interface at an angle greater than the critical angle so that total internal reflection occurs.

Total internal reflection

Snell's Law

$$\frac{n_1}{n_2} = \frac{\sin\theta_2}{\sin\theta_1}$$

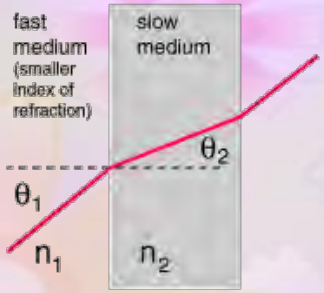

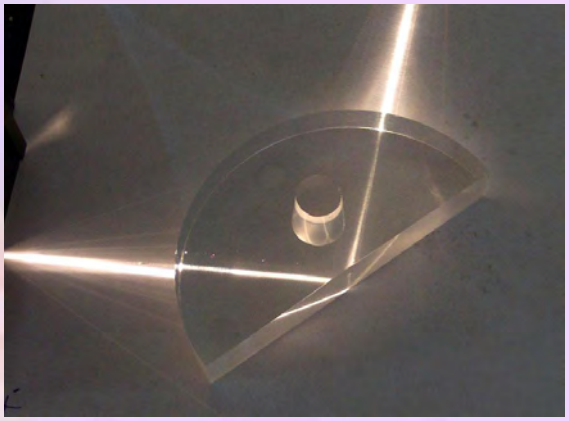

Total internal reflection

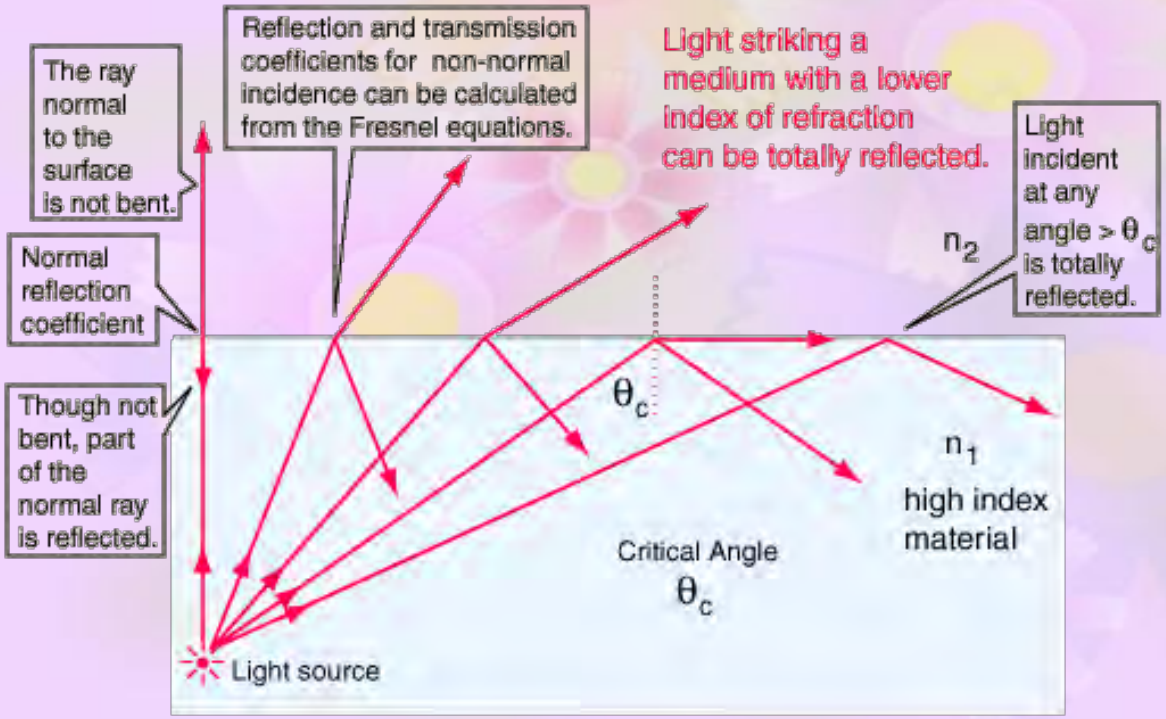

$$\theta_c = \sin^{-1}(n_2/n_1)$$

Penetration depth of evanescent wave

The penetration depth (d_p) into the sample is typically between 0.5 and 2 um, with the exact value being determined by the wavelength of light (λ), the angle of incidence (θ) and the indices of refraction for the ATR crystal (n_1) and the medium (n_2) being probed.[2]

$$d_p = \frac{\lambda}{2\pi n_1 (\sin^2\theta - n_{21}^2)^{1/2}}$$

where

$$n_{21} = n_2/n_1$$

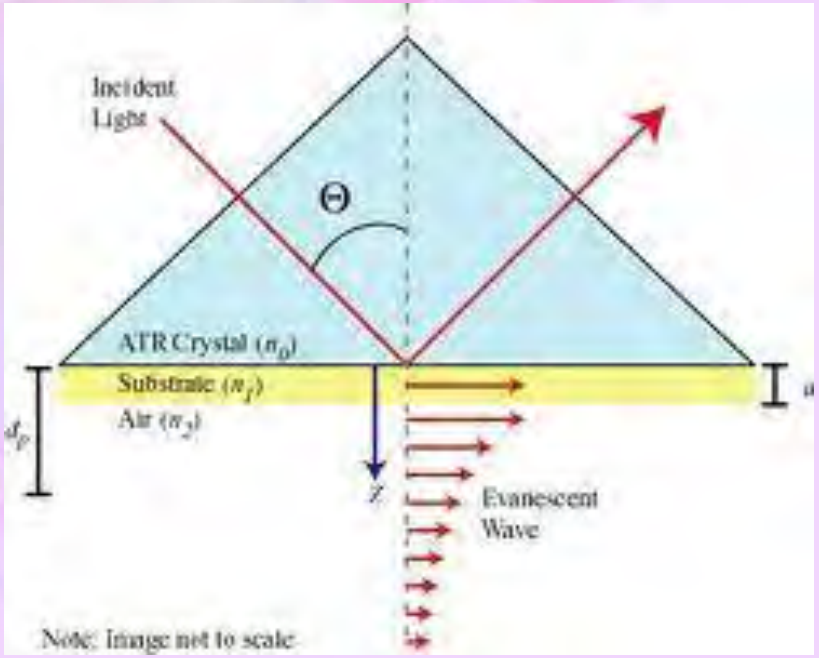

Evidence and applications of ATR

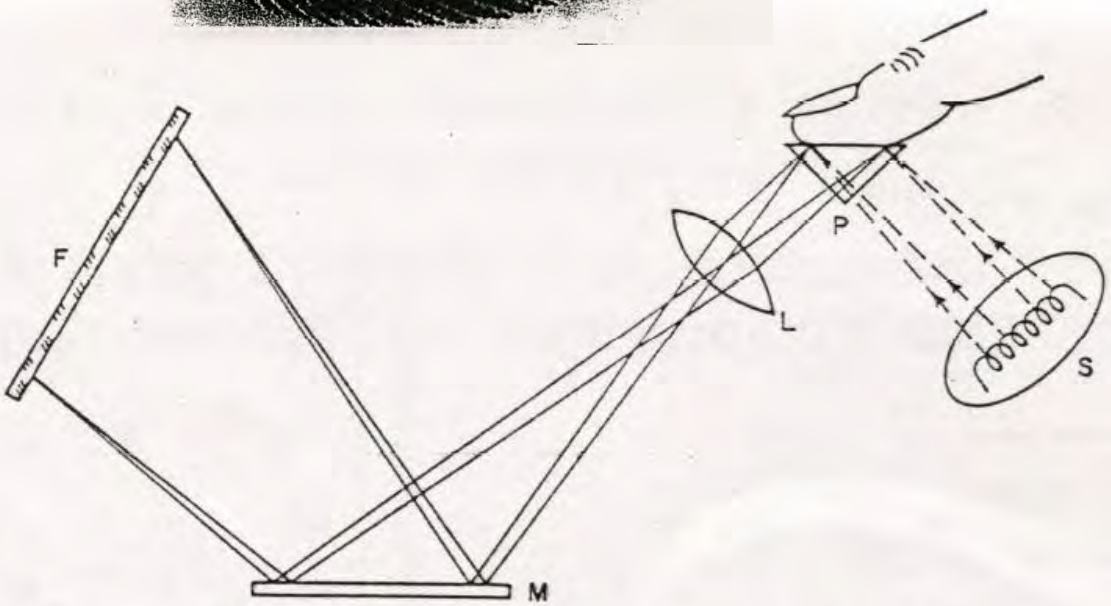

Fig. 2. Schematic diagram of inkless fingerprint recording instrument. The finger is pressed against the hypotenuse of the prism (P) illuminated by the light source (S) and imaged onto the screen or photofilm (F) by the lens (L) and mirror (M). Total reflection is destroyed only where contact is made between the skin and the prism, i.e., at the ridges but not at the valleys, and thus a high contrast image of surface reliefs is obtained.

Fingerprints on a glass of water made visible by frustrated total internal reflection

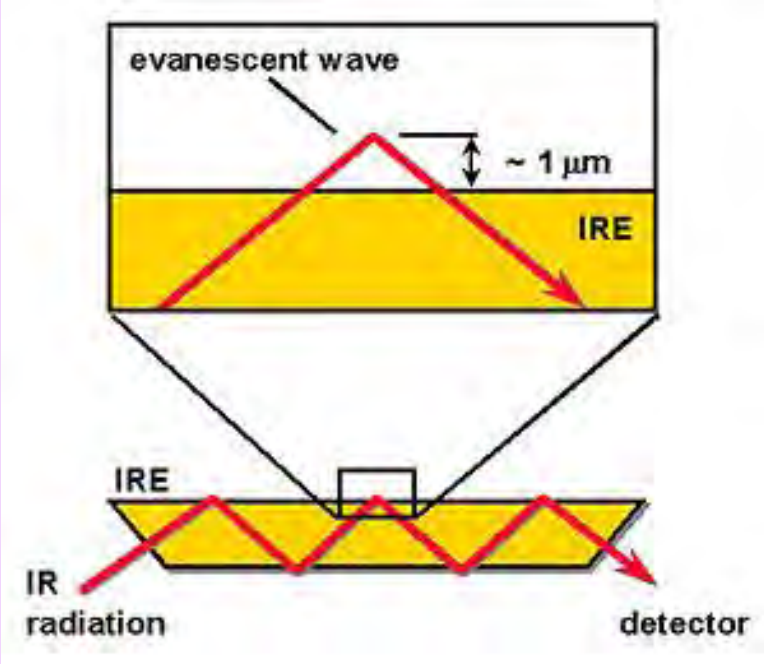

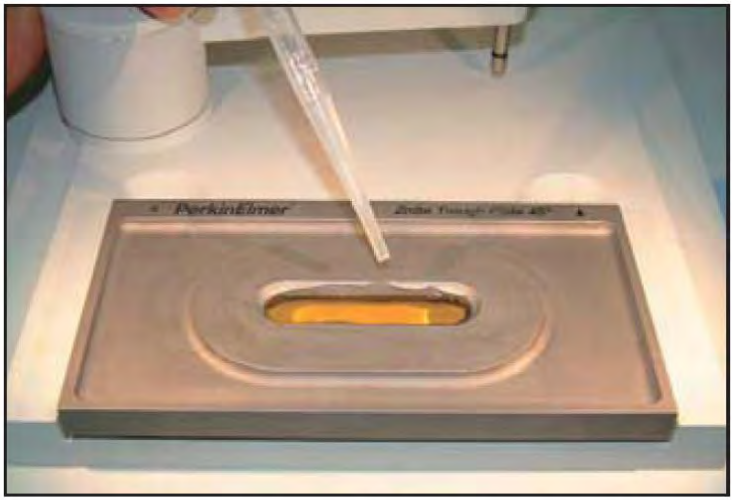

Figure 5. Using a pipette to add a liquid sample to a ZnSe HATR trough plate.

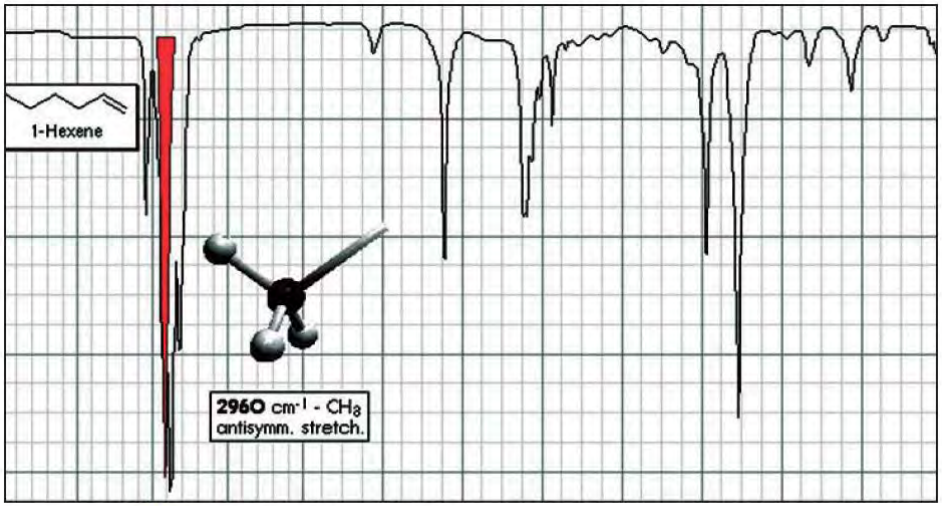

Figure 1. A Mid-Infrared spectrum of Hexene.

http://las.perkinelmer.com/content/TechnicalInfo/TCH_FTIRATR.pdf

The Beer's law

$$T = \frac{I}{I_0} = 10^{-\alpha \ell} = 10^{-\varepsilon \ell c}$$

$$A = -\log_{10}\left(\frac{I}{I_0}\right)$$

$$A = \varepsilon \ell c = \alpha \ell$$

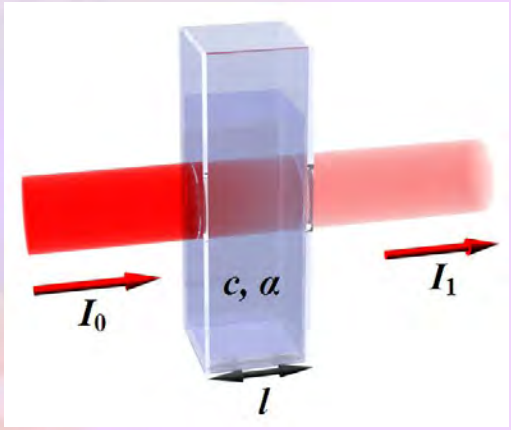

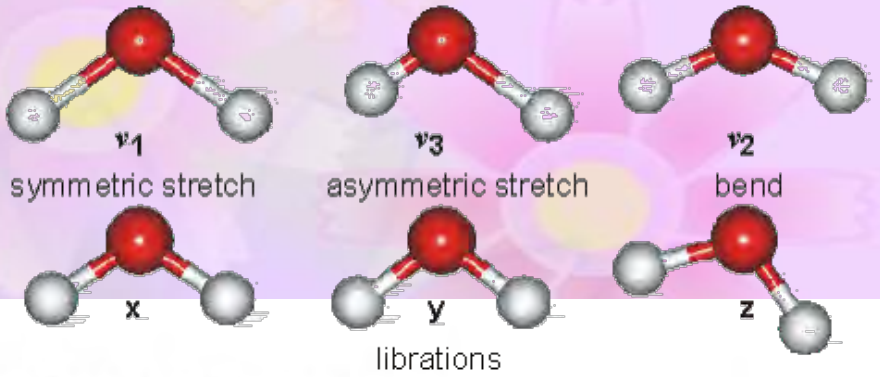

The vibrational spectra of liquid water

Main vibrations of liquid ordinary and heavy water

Vibration(s) [942]	liquid H_2O (25°C)		liquid D_2O (25°C)	
	ν, cm^{-1}	E_0, $M^{-1}\,cm^{-1}$	ν, cm^{-1}	E_0, $M^{-1}\,cm^{-1}$
ν_2	1643.5	21.65	1209.4	17.10
combination of ν_2+ libration	2127.5	3.46	1555.0	1.88
ν_1, ν_3 , and overtone of ν_2	3404.0[e]	100.61	2504.0	69.68

Biological applications of ATR

•Total internal reflection fluorescence (TIRF) microscope

The development of the microscope aims to imaging molecular events occurring on cellular surfaces such as cell adhesion, binding of cells by hormones, secretion of neurotransmitters, and membrane dynamics.

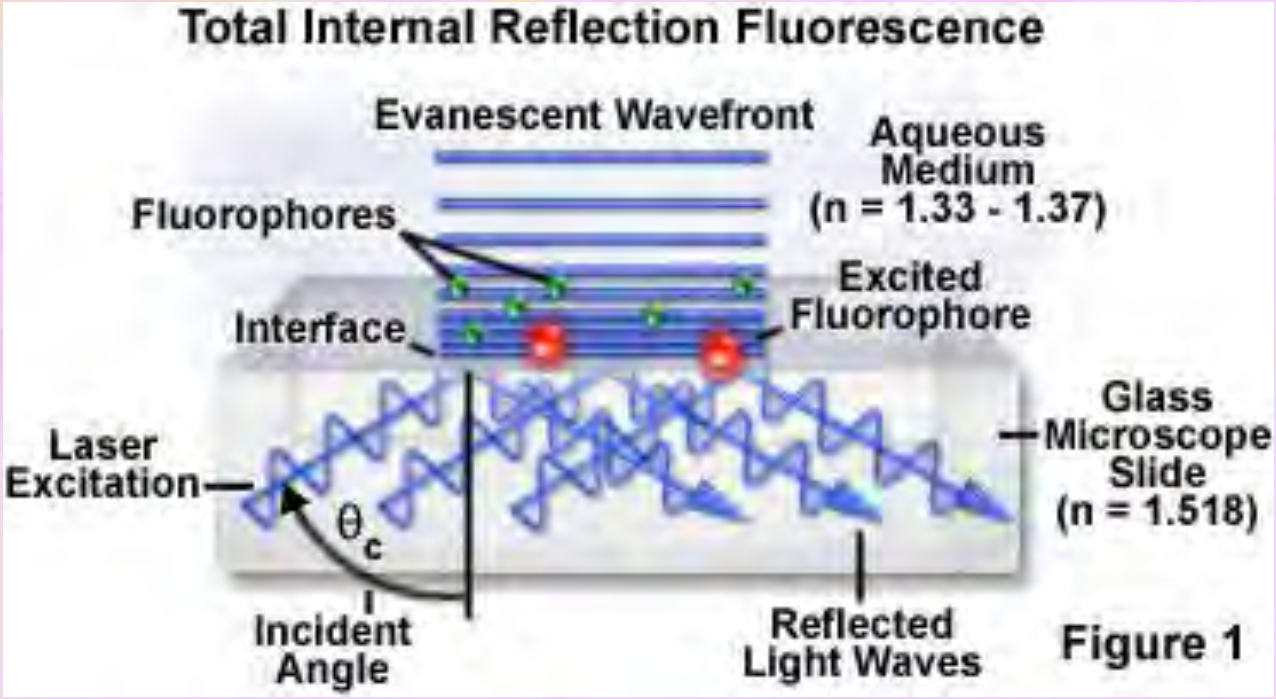

TIRF microscopy

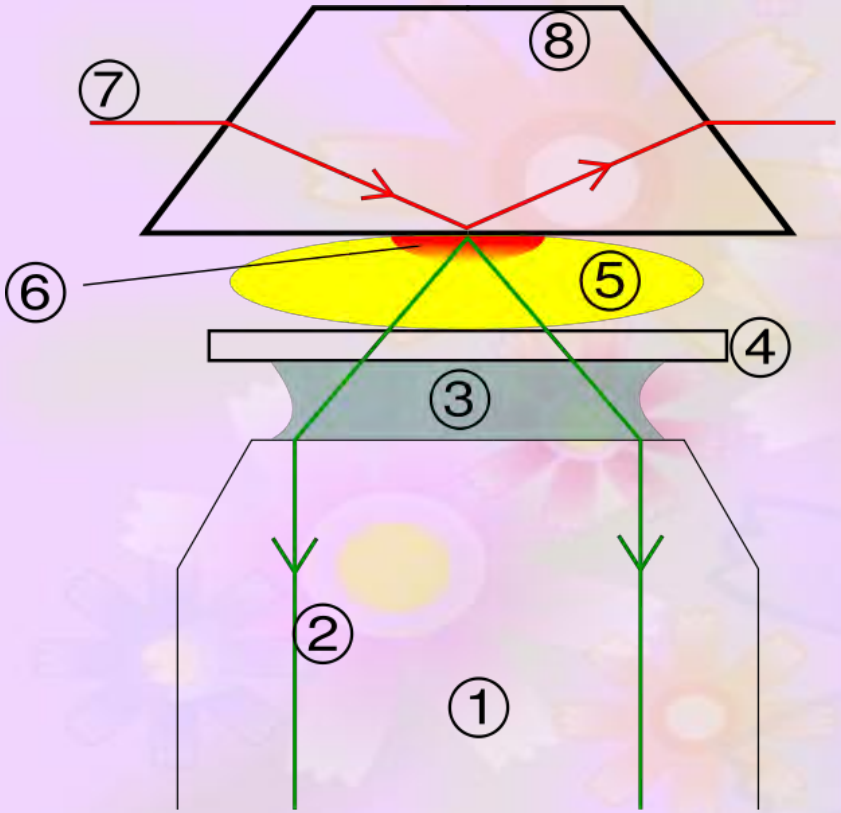

1. Objective
2. Emission beam (signal)
3. Immersion oil
4. Cover slip
5. Specimen
6. Evanescent wave range (<200 nm)
7. Excitation beam
8. Quartz prism

Advantages of TIRF microscopy

In cell and molecular biology, a large number of molecular events occur on cellular surfaces such as cell adhesion, binding of cells by hormones, secretion of neurotransmitters, and membrane dynamics. However, when these molecules are excited and detected with a conventional fluorescence microscope, the resulting fluorescence from those fluorophores bound to the surface is often overwhelmed by the background fluorescence due to the much larger population of non-bound molecules.

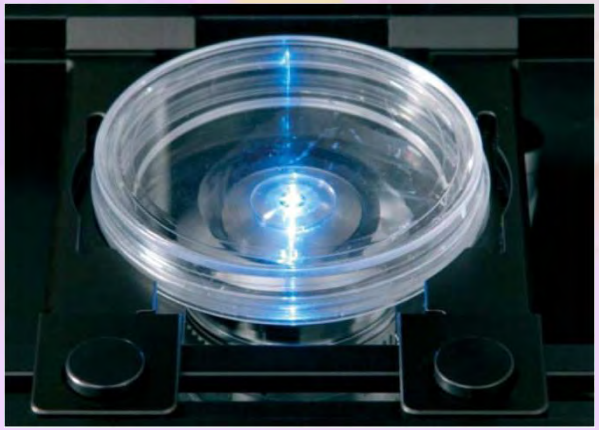

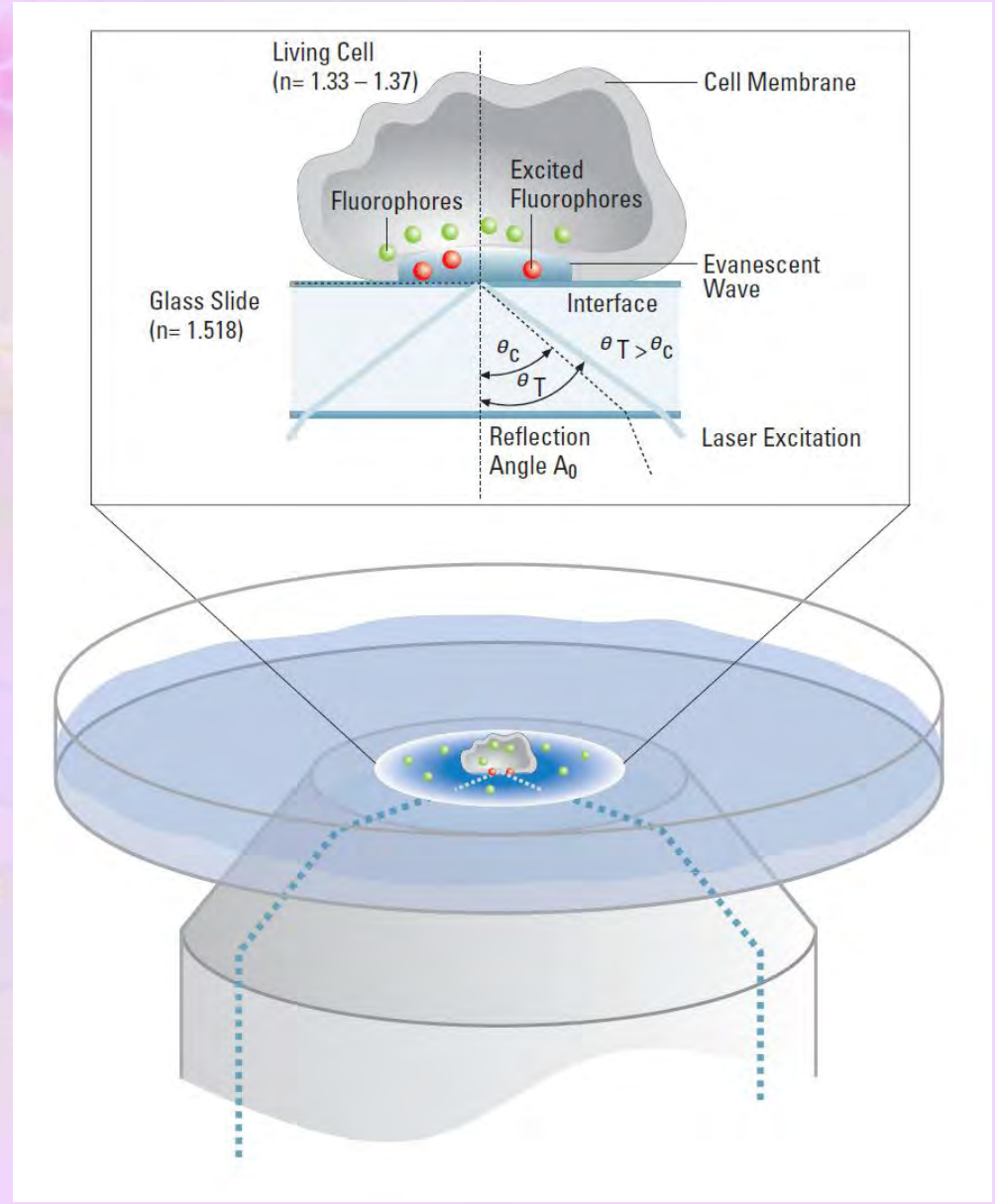

Impact: I25.1 Biosensor analysis

- **biosensor analysis,** the detection of changes in the optical properties of a surface in contact with a biopolymer.
- **plasma,** a dense gas of charged particles.
- **plasmons,** oscillations in electron density.
- **evanescent wave,** an oscillation in electron density that propagates away from a surface.
- **surface plasmon resonance,** the absorption of energy from an incident beam of electromagnetic radiation by surface plasmons.

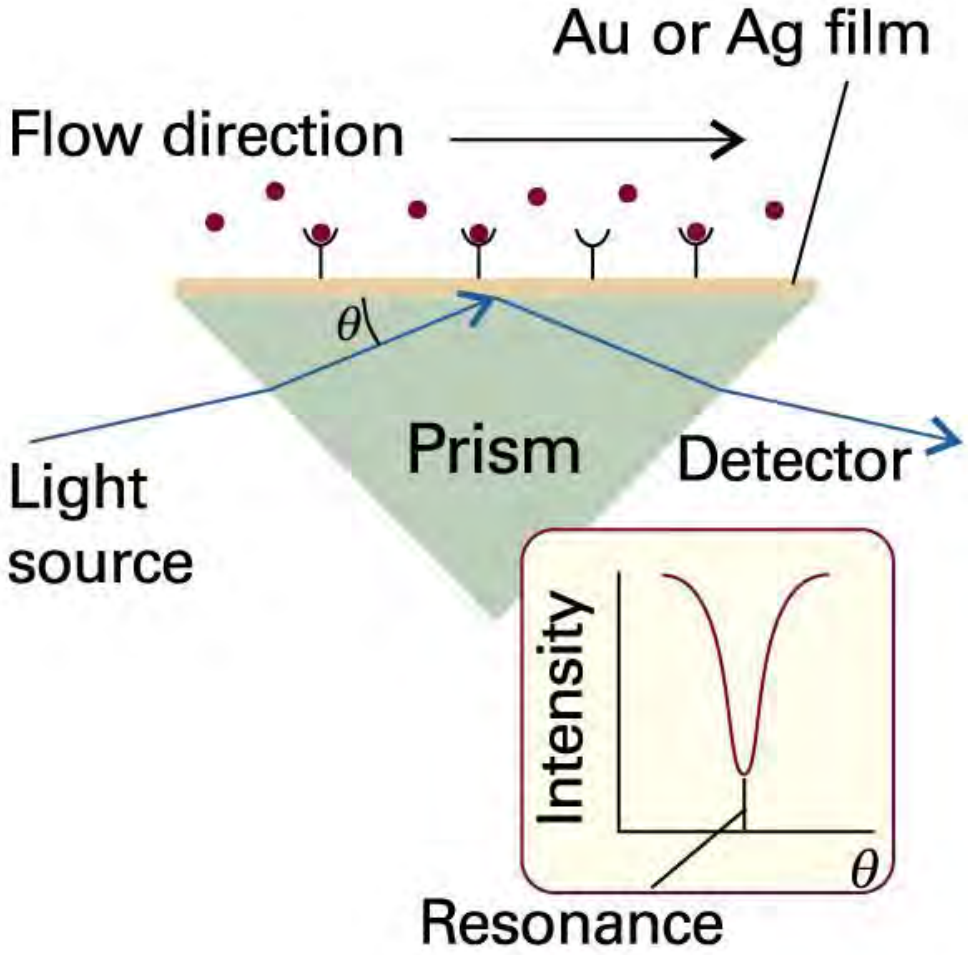

Fig. 25.26 The experimental arrangement for the observation of surface plasmon resonance, as explained in the text.

Principle of surface plasma resonance (SPR)

The incident wave vector is given by the following expression:

$$K_i = \left(\frac{2\pi}{\lambda}\right) n \sin\theta_i$$

where K_i is a component of the incident light wave vector parallel to the prism Interface, θ_i is the incident light angle, λ is the wavelength of the incident light and n is the refractive index of the prism.

The wave vector of the plasmon mode is described by the following expression

$$K_P = \left(\frac{2\pi}{\lambda}\right)\sqrt{\frac{\varepsilon_1\varepsilon_2}{\varepsilon_1+\varepsilon_2}}$$

where K_p is the surface plasmon wave vector and ε_1 and ε_2 are the complex dielectric constants of the metal film and the dielectric exit medium, respectively.

Smith *et al.* Appl. Spectrosc. **57**, 320A (2003)

SPR occurs when $K_i = K_p$

The intensity of the reflected light will decrease where SPR exists, thereby giving rise to a well defined minimum in the reflectance intensity.

- If the incident angle is fixed and polychromatic and light is reflected from the surface, then light will be adsorbed by the resonance at particular wavelengths giving rise to a typical SPR minimum in the reflectance spectrum.

- If monochromatic light is reflected from the surface over a range of incident angles, then a similar reflectance minimum will occur with respect to the incident angle.

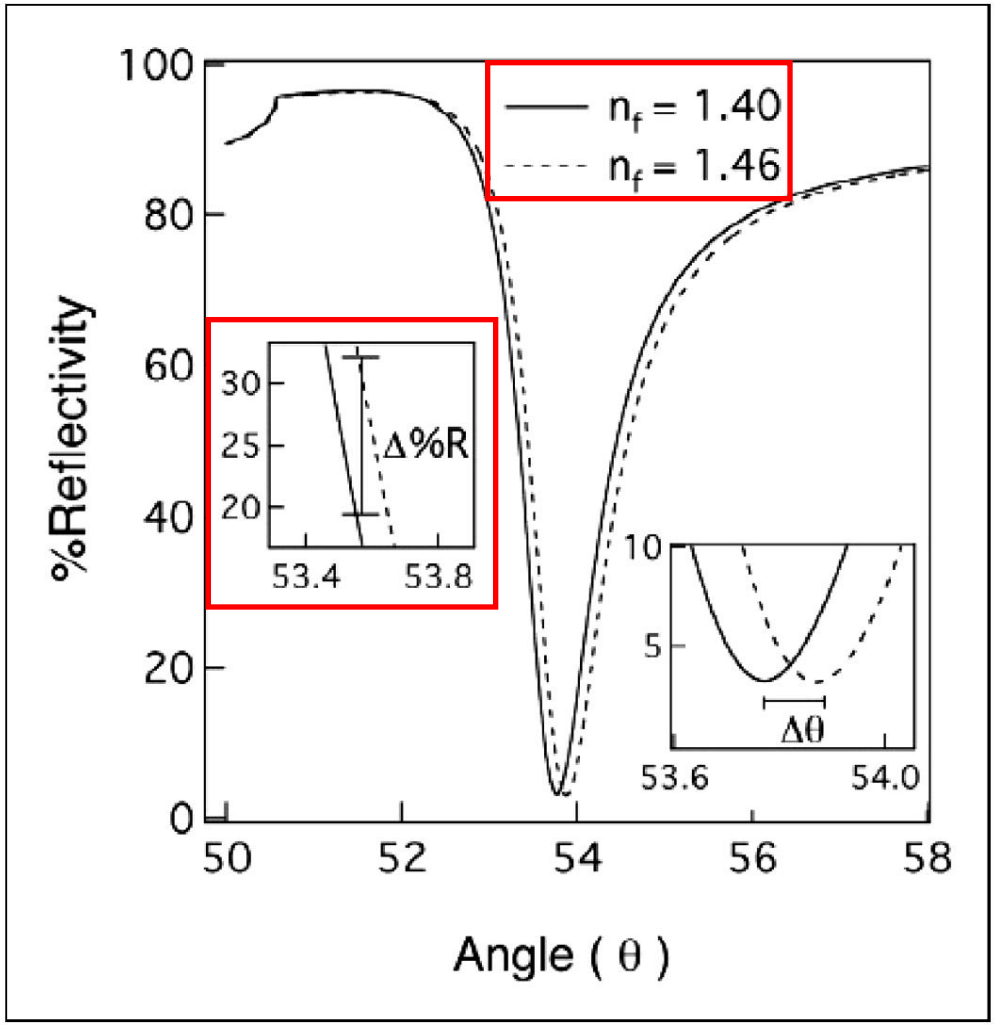

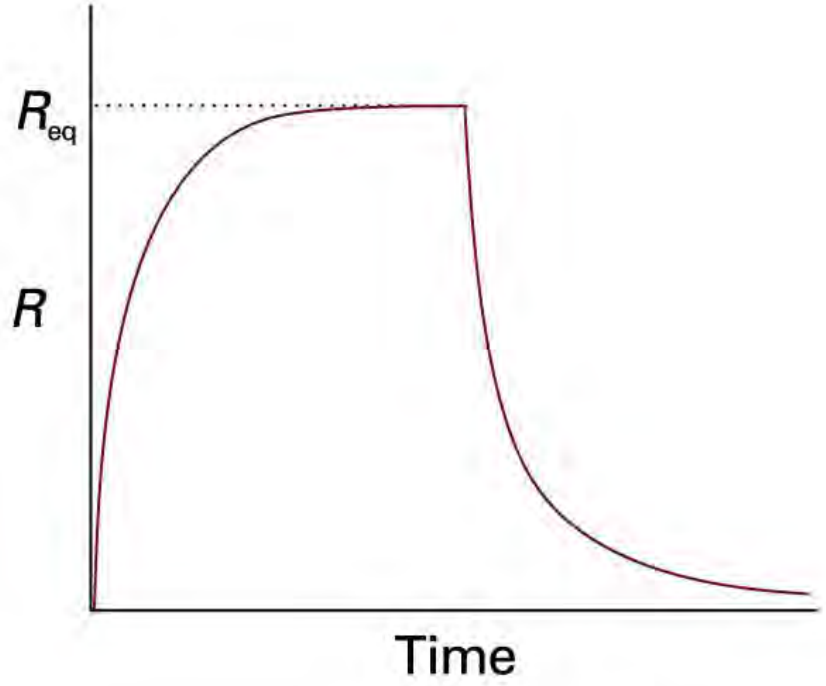

Fig. 25.27 The time dependence of a surface plasmon resonance signal, R, showing the effect of binding of a ligand to a biopolymer adsorbed on to a surface. Binding leads to an increase in R until an equilibrium value, R_{eq}, is obtained. Passing a solution containing no ligand over the surface leads to dissociation and decrease in R.

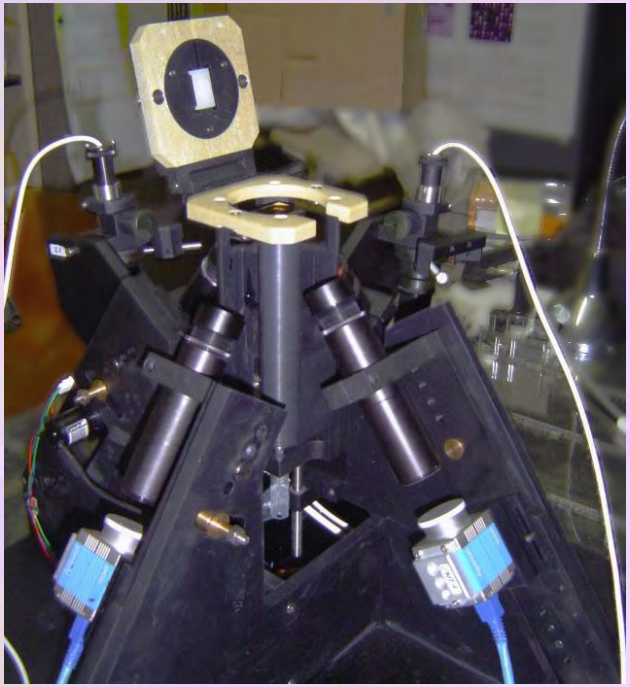

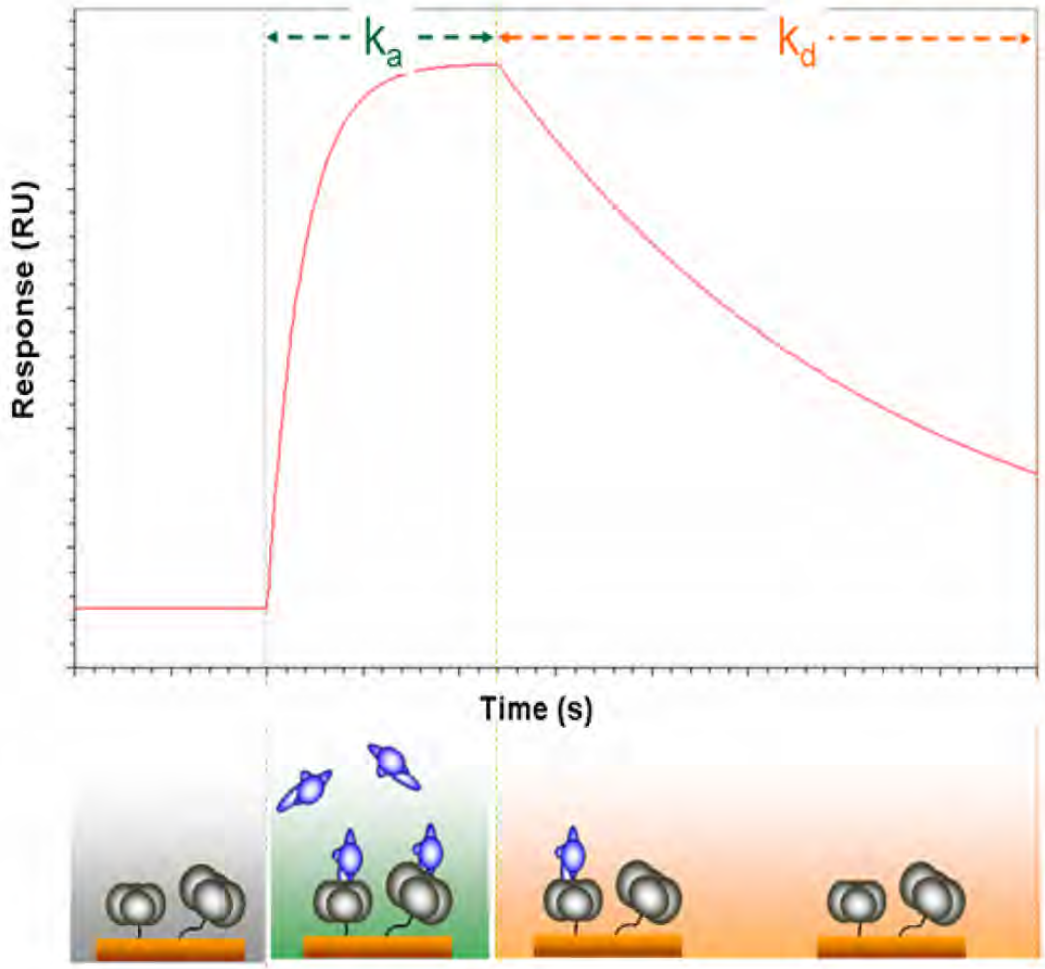

Analyte Mass Transport

$$A_0 \overset{k_m}{\Leftrightarrow} A$$

The concentration of analyte at the surface (***A***) is related to the concentration of injected analyte (***A₀***) by k_m, the mass transport coefficient.

Complex (*AB*) Formation

$$A + B \underset{k_d}{\overset{k_a}{\Leftrightarrow}} AB$$

Where the forward (on) and reverse (off) rates are k_a and k_d, respectively.

http://www.labtech.co.uk/downloads/nomadics_principles.pdf

PROCESSES AT ELECTRODES

25.8 The electrode–surface interface

- **electrical double layer,** a sheet of one charge at the surface of the electrode and a sheet of opposite charge next to it in the solution.
- **Galvani potential difference,** the potential difference between the bulk of the metal electrode and the bulk of the solution.
- **Helmholtz layer model,** a model of the double layer in which the solvated ions arrange themselves along the surface of the electrode but are held away from it by their hydration spheres.

25.8 The electrode–surface interface (cont..)

- **outer Helmholtz plane** (OHP), the outer sheet of charge.
- **inner Helmholtz plane** (IHP), the inner sheet of charge.
- **Gouy–Chapman model,** a model of he double layer in which the outer layer is diffuse.
- **diffuse double layer,** an inner layer of charge and an outer ionic diffuse atmosphere.
- **Stern model,** a model of the double layer in which the ions closest to the electrode are constrained into a rigid plane while outside that plane the ions are dispersed as in the Gouy–Chapman model.

The electrode-surface interface

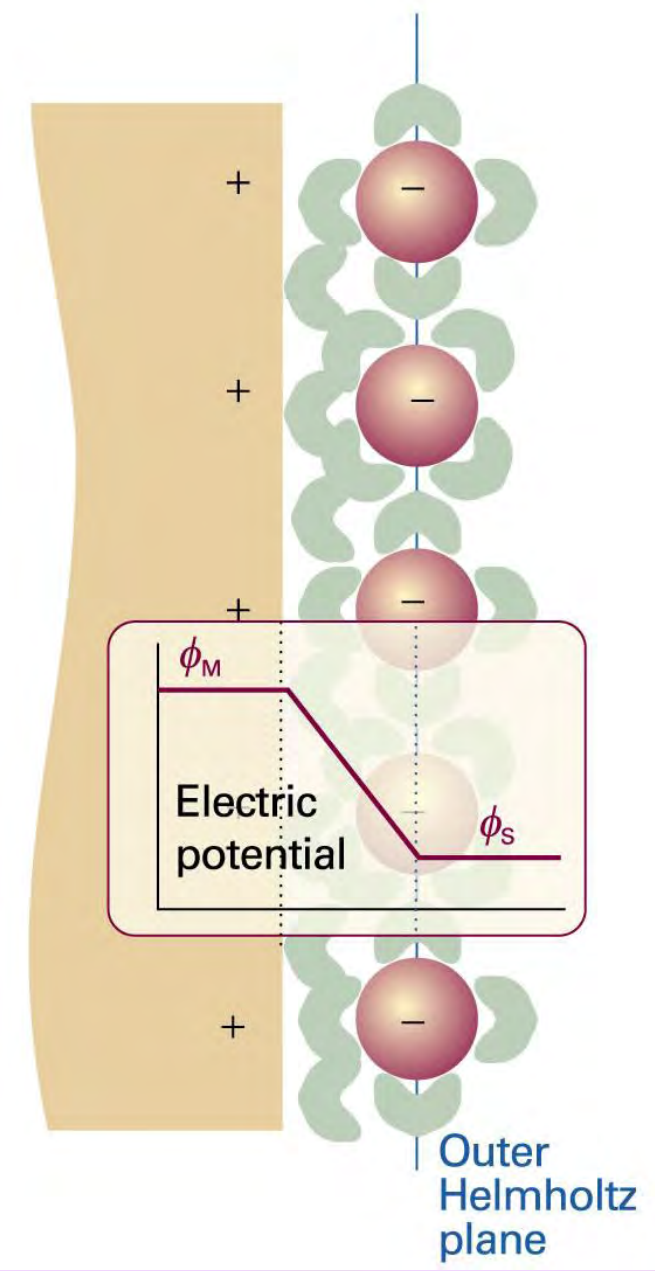

Fig. 25.30 A simple model of the electrode–solution interface treats it as two rigid planes of charge. One plane, the outer Helmholtz plane (OHP), is due to the ions with their solvating molecules and the other plane is that of the electrode itself. The plot shows the dependence of the electric potential with distance from the electrode surface according to this model. Between the electrode surface and the OHP, the potential varies linearly from φ_M, the value in the metal, to φ_S, the value in the bulk of the solution.

The electrode-surface interface

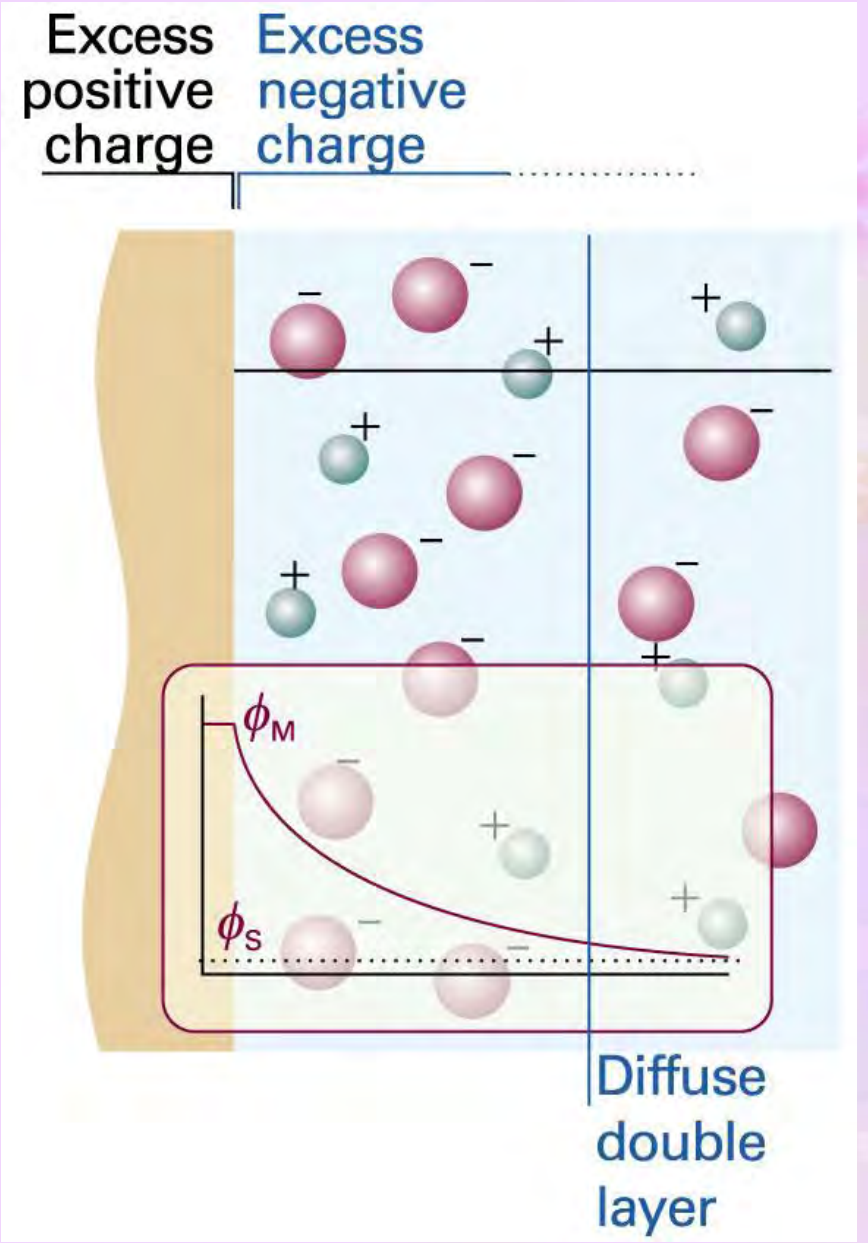

Fig. 25.31 The Gouy–Chapman model of the electrical double layer treats the outer region as an atmosphere of counter-charge, similar to the Debye–Hückel theory of ion atmospheres. The plot of electrical potential against distance from the electrode surface shows the meaning of the diffuse double layer (see text for details).

The electrode-surface interface

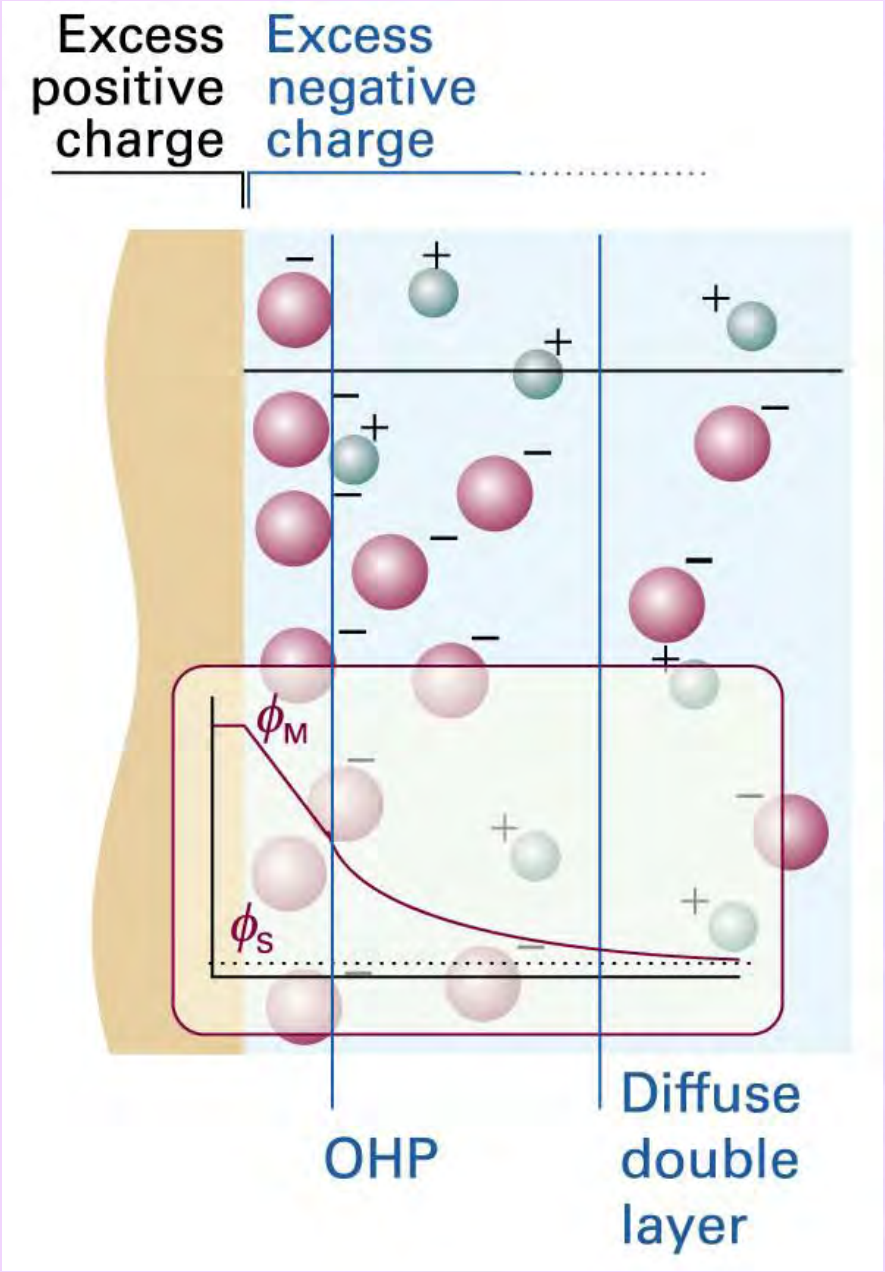

Fig. 25.32 A representation of the Stern model of the electrode–solution interface. The model incorporates the idea of an outer Helmholtz plane near the electrode surface and of a diffuse double layer further away from the surface.

Zeta potentials of colloids

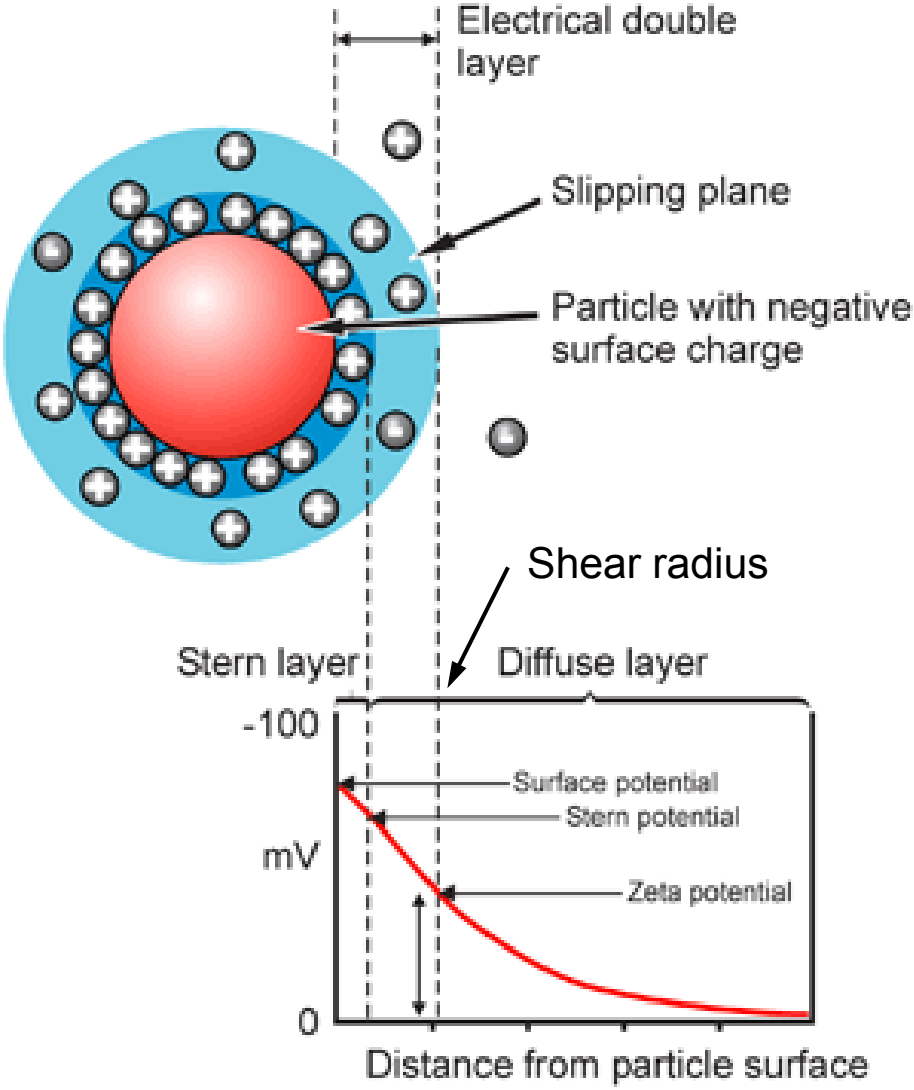

- The zeta potential is the electric potential at the radius of shear relative to its value in the distant, bulk medium.

- The radius of shear is the radius of the sphere that captures the rigid layer of charge attached to a colloid particle.

http://www.malvern.com/LabEng/technology/zeta_potential/zeta_potential_LDE.htm

What is zeta potential?

•Most particles dispersed in an aqueous system will acquire a surface charge, principally either by ionization of surface groups, or adsorption of charged species.

•These surface charges modify the distribution of the surrounding ions, resulting in a layer around the particle that is different to the bulk solution.

•If the particle moves, under Brownian motion for example, this layer moves as part of the particle.

•The zeta potential is the potential at the point in this layer where it moves past the bulk solution. This is usually called the slipping plane.

•In other words, zeta potential is the potential difference between the dispersion medium and the stationary layer of fluid attached to the dispersed particle.

•Zeta potential is one of the main forces that mediate interparticle interactions. The significance of zeta potential is that its value can be related to the stability of colloidal dispersions.

•Particles with a high zeta potential of the same charge sign, either positive or negative, will repel each other. Colloids with high zeta potential (negative or positive) are electrically stabilized while colloids with low zeta potentials tend to coagulate or flocculate.

Zeta potential [mV]	Stability behavior of the colloid
from 0 to ±5,	Rapid coagulation or flocculation
from ±10 to ±30	Incipient instability
from ±30 to ±40	Moderate stability
from ±40 to ±60	Good stability
more than ±61	Excellent stability

The zeta potential is sensitive to the concentration and type of ions (such as pH) in solution.

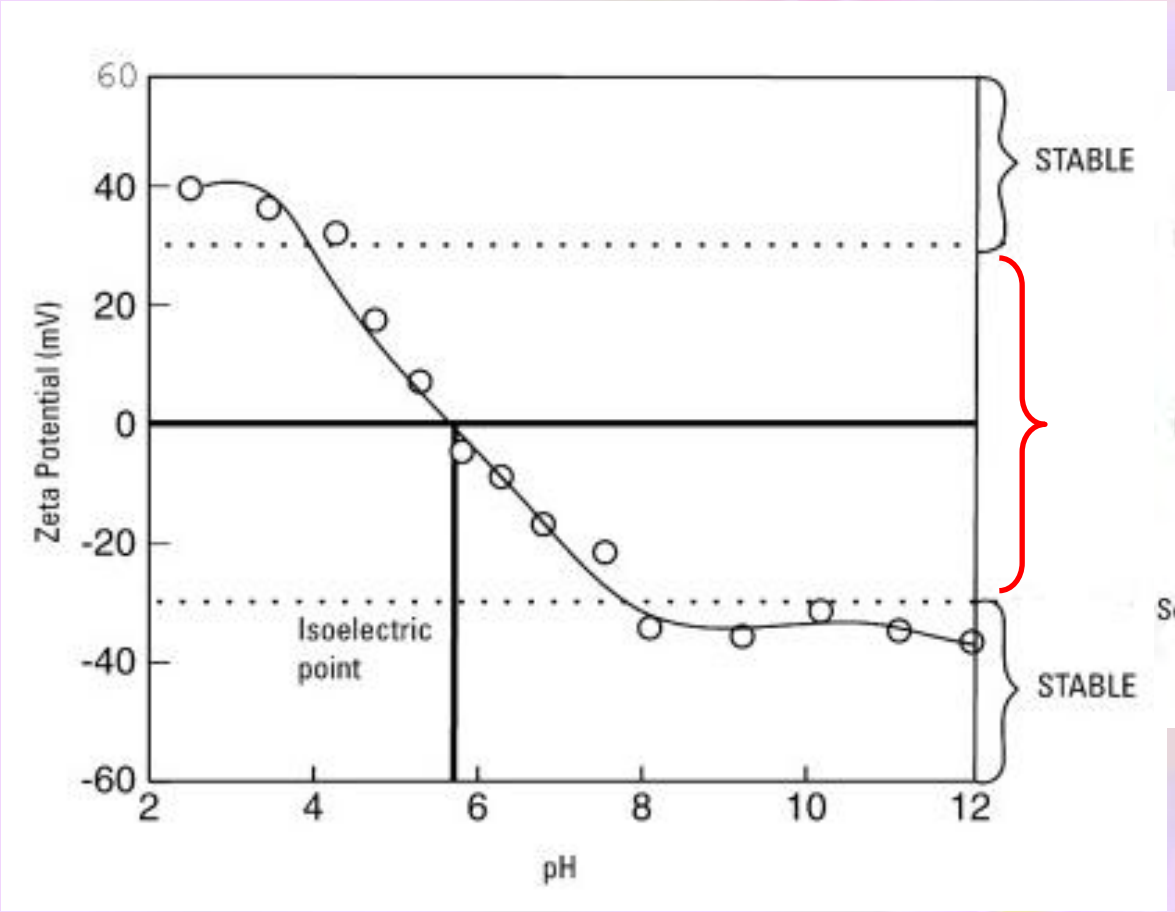

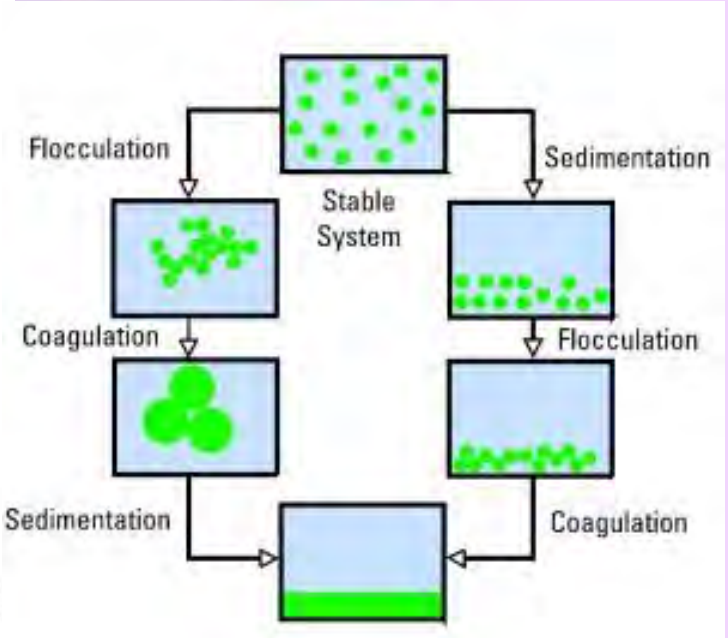

Laser Doppler Velocimetry

•Laser beams are aligned at the stationary layer in the cell.
•At the crossing point of the beams, Young's interference fringes of known spacing are formed.
•Particles moving through the fringes under the influence of the applied electric field scatter light whose intensity fluctuates with a frequency that is related to the particles velocity.
•A frequency spectrum is produced from which the mobility and hence zeta potential are calculated